Petroleum Science 23 (2026) 2863–2884

Contents lists available at ScienceDirect

Petroleum Science

journal homepage: www.keaipublishing.com/en/journals/petroleum-science

Original Paper

Gas-solid two-phase flow erosion of needle throttle valve in shale gas field based on CFD-DEM model

Bing-Yuan Hong [a,b,c], Zhe Wu [a], Yan-Bo Li [d], Yu Meng [e], Yue Su [a], Wei-Dong Li [f], Bai-Kang Zhu [a], Xian-Lei Chen [g], Wei-Qiang Wang [a], Dai-Wei Liu [a,*]

[a] National & Local Joint Engineering Research Center of Harbor Oil & Gas Storage and Transportation Technology/Zhejiang Key Laboratory of Petrochemical Environmental Pollution Control/Zhejiang Key Laboratory of Pollution Control for Port-Petrochemical Industry, School of Petrochemical Engineering & Environment, Zhejiang Ocean University, Zhoushan, 316022, Zhejiang, China
[b] Chongqing University Industrial Technology Research Institute, Chongqing, 400030, China
[c] College of Safety and Ocean Engineering, China University of Petroleum (Beijing), Beijing, 102249, China
[d] Beijing Gas Group Co., Ltd., Beijing, 100062, China
[e] Zhejiang Heng An Tai Petroleum Engineering Co., Ltd., Zhoushan, 316013, Zhejiang, China
[f] College of Chemical Engineering, Fuzhou University, Fuzhou, 350116, Fujian, China
[g] Zhoushan Institute of Calibration and Testing for Qualitative and Technical Supervision, Zhoushan, 316013, Zhejiang, China

ARTICLE INFO

Article history:
Received 1 January 2025
Received in revised form
27 January 2026
Accepted 27 January 2026
Available online 5 February 2026

Edited by Meng-Jiao Zhou

Keywords:
Shale gas field
Needle throttle valve
Gas-solid two-phase flow
Particle flow erosion
CFD-DEM coupling calculation

ABSTRACT

Needle throttle valve (NTV) is a key equipment to ensure the safe production of shale gas fields, but it is often seriously eroded by the solid particles in the produced gas. At this work, the CFD-DEM coupling calculation method is adopted to investigate the internal flow field characteristics and the erosion rate of each component of the NTV under gas-solid two-phase flow. The accuracy of the numerical model is validated by the comparison results of simulation and experiment. The results show that with the increase of particle diameter, the maximum erosion rate of each part of the valve generally increases. When valve opening degree (VOD) is equal to 0.5, it has the best effect on suppressing erosion rates at high flow velocity. There is a "vulnerable zone" of the spool cone that is not affected by the changes in particle diameter and VOD, which occupies 2/3 of the height of the spool cone. This work not only predicts the vulnerable zone of each component of the valve, but also reveals the erosion mechanism of the NTV, and can provide a reference for the design and maintenance of the valve.

1. Introduction

With the widening energy gap and advances in extraction technology, the development of shale gas has become a hotspot. It has been described as a game changer due to its potential role in addressing global climate change, protecting the security of energy, and revitalizing local economies (Tan et al., 2022; Knudsen and Foss, 2017). The development of shale gas requires the installation of a throttling device at the wellhead. The needle throttle valve (NTV) is a commonly used key component for throttling, acting as a crucial link connecting the underground gas field and the above ground gathering and transmission system. The back pressure and flow rate can be controlled by adjusting the valve opening degree to prevent accidents such as overflow, well surge or even blowout.

As shale gas is often extracted using hydraulic fracturing technology, solid particles are frequently carried in the extracted gas flow. Although most shale gas fields now adopt downhole sand fixation measures, the extracted shale gas still inevitably contains a large number of solid particles (Hong et al., 2020). For example, the solid sand production of a gas well in the Changning shale gas field can be as high as 10 t/d (Jia et al., 2021). These solid particles are carried by the high-velocity gas flow and continuously impact the throttle valve (Wang et al., 2021), resulting in the removal of the internal material of the valve and the loss of mass and thickness, which is known as erosion wear (Neilson and Gilchrist, 1968). The valve failure forms caused by erosion primarily include seal

* Corresponding author.
E-mail address: daiwei@zjou.edu.cn (D.-W. Liu).
Peer review under the responsibility of China University of Petroleum (Beijing).

https://doi.org/10.1016/j.petsci.2026.01.043

Nomenclature

ave	Average value
CFD	Computational fluid dynamics
D_p	Particle diameter, m
DPM	Discrete phase method
DEM	Discrete element method
ER	Particle erosion rate, μm/s
E^*	Equivalent Young's modulus, Pa
F	Force, N
H_v	Vicker's hardness, GPa
max	Maximum value
NTV	Needle throttle valve
p	Static pressure, Pa
R^*	Equivalent radius, m
Stk	Stokes number
u	Flow velocity, m/s
VOD	Valve opening degree
α	Particle impact angle, °
ρ	Density, kg/m^3
μ	Molecular viscosity of the fluid, Pa·s
τ_r	The relaxation time of the particle, s

failure, flow control inaccuracy and spool motion stagnation, etc. Compared with the straight pipe, elbows and tee pipe, NTV has a more complex internal structure which can lead to particle aggregation and high-frequency impact on the wall. Therefore, it is of great significance to study the erosion model of NTV to reveal the failure mechanism and avoid the accidents caused by perforation, fracture and leakage to ensure the flow safety in shale gas fields. This paper utilizes the CFD-DEM model to study the erosion of NTV with gas-solid two-phase flow in shale gas fields.

Gas-solid two-phase flow erosion is a very complex multi-physics process, which is usually investigated using experimental and numerical simulations. Most studies have focused on macro-parameters to determine the erosion results and have used micro-parameters to deepen the understanding of the flow field and particle motion mechanisms.

In terms of experimental research, various techniques have been applied. Wang et al. (2019) investigated the near-wall flow velocity and particle impact velocity in fluids using particle image velocimeter (PIV) and particle tracking velocimeter (PTV) techniques. Lin et al. (2015, 2018) found that smaller sand particles often do not reflect enough light resulting in the PTV device having a higher accuracy than the PIV device in measuring high velocity, small particle size flow fields. Zhang et al. (2015) used a 3D scanner to accurately measure the wall thickness variation of an eroded specimens. Our team has also constructed a novel experimental equipment. Based on this equipment and with the aid of scanning electron microscopy, the erosion characteristics of different kind of steels in gas-solid two-phase flow were investigated (Hong et al., 2022). It was found that steel erosion was most severe at an impact angle of 30° and a model with low tolerance (<3%), highly feasibility and strong consistency was proposed to accurately predict erosion for different steels. However, while experiments provide direct results, they are limited in obtaining the distribution of the gas flow field and transient particle movement information, especially for complex structures like the NTV.

Numerical simulation methods have thus been developed as a crucial complement. CFD-DPM is one of the most primary methods for studying particle erosion problems in gas-solid two-phase flow (Vieira et al., 2016). Wallace et al. (2004) investigated the erosion of valve components in water slurry flow using the Euler-Lagrange flow model and the results showed that theoretical derivation alone leads to a significant underestimation of erosion rates. Subsequently, Mazur et al. (2004) used CFD-DPM to investigate solid particle erosion in the bypass valve of a steam turbine main shut-off valve and improved the design of the valve, resulting in a 51% reduction in the erosion rate. Zhu et al. (2019) used CFD-DPM to reveal the erosion mechanism of a U-bend by a sand-laden oil stream. Our team has also established an CFD-DPM model and verified the reliability of the proposed numerical model by comparing the predicted data with the experimental data. On this basis, the effects of important factors such as flow rate, particle mass flow rate, particle diameter, sand shape factor, pipe diameter, radius of curvature of elbow on the maximum erosion rate were investigated separately for the wearing parts during the pneumatic conveying process, such as 90° elbows, right-angled pipe and blind tee (Hong et al., 2021a, 2021b, 2023). The study can provide a theoretical basis for the selection of the pipe fitting structure under different industrial conditions thereby reducing the erosion rate of pipe, improving the integrity of pipeline management, prolonging the service life and ensuring the safety of flow.

However, the CFD-DPM method is typically limited to dilute phase (low particle concentration) gas-solid two-phase flows. It simplifies the physics by using normal and tangential rebound coefficients and ignores particle-particle collisions and the void ratio in the fluid equation. The flow path within the NTV is highly complex and variable, and the throttling process can lead to dense particle conditions (high sand content, small particle diameter), where inter-particle collision, local accumulation, and deposition are severe (Xu et al., 2016; Chen et al., 2015; Li et al., 2024). Under such conditions, the traditional CFD-DPM two-way coupling method can lead to significant errors (Xu et al., 2022).

Therefore, the CFD-DEM four-way coupling method, which rigorously accounts for particle-particle, particle-gas flow, and particle-wall interaction forces, has emerged as a very promising and accurate approach for high-concentration flows (Lin et al., 2020). The DEM method is based on Newton's second law to solve the particles, and different particle force models can give different characteristics to the particles, which can greatly improve the accuracy of the calculation at the condition of high particle density. However, the DEM consumes more computational resources as it not only has to search the surrounding particles when dealing with particle collisions but also the short time step size required for the explicit time integration. Xu et al. (2016) and Chen et al. (2015) used a variety of coupled computational methods on the elbow with experimental control studies. The results have shown that the use of the CFD-DEM coupling method in the calculation of high particle concentration conditions have obvious accuracy advantages. Li et al. (2024) used the CFD-DEM coupling method to simulate a vertical-curved-horizontal pipe, and the results showed that the concentration of solid particles on the center of the vertical pipe increased with the decrease of particle sphericity. Xu et al. (2022) used the CFD-DEM coupling method to reveal the erosion mechanism of the inner surface of a ball valve under liquid-solid two-phase flow and found that the formation of a protective layer near the wall is the result of the aggregation of particles. Lin et al. (2020, 2022) also used CFD-DEM coupling method to investigate the erosion mechanism of gate valve under gas-solid two-phase flow, and the results showed that the number of particles plays an important role in erosion.

Despite the importance of NTVs in shale gas extraction and the complex flow regime they experience, the flow characteristics of the NTV under gas-solid two-phase flow conditions are still unclear, and the detailed characteristics of particle dynamics

(velocity, direction, impact, etc.) during the throttling process lack in-depth study. Specifically, no comprehensive CFD-DEM study has been reported for the erosion mechanism within the NTV, which is a key component operating under potentially high particle concentration in shale gas extraction.

To address this critical gap and enhance the integrity of flow control in shale gas fields, this paper adopts the advanced CFD-DEM approach to systematically investigate the erosion of the NTV. The numerical model is first validated against multiple sets of experimental and simulation data. The main contributions of this paper are outlined as follows:

(1) A CFD-DEM gas-solid two-phase flow erosion model for NTV is constructed. By comparing the results with the CFD-DPM method, we demonstrate the superiority of the CFD-DEM method in computational accuracy for the complex flow within the NTV.
(2) A specific "vulnerable zone" is identified on the valve cone. We reveal that this critical zone, which occupies 2/3 of the height of the spool cone, is independent of the valve opening degree and particle diameter, providing a key insight for design optimization.
(3) The erosion mechanism of gas-solid two-phase flow in the NTV is revealed by systematically analyzing parameters such as the gas flow field, particle distribution, particle trajectory, average erosion rate, and maximum erosion rate of each valve part.

The research results can provide a crucial theoretical reference for the optimal design of NTVs (e.g., material selection, structural improvements for the "vulnerable zone") and inform on-site maintenance strategies in shale gas fields.

2. Problem description

The NTV studied at this work shows in Fig. 1. In this model, a gas stream entrained with particles enters the valve. After passing through the upstream pipe section, the gas-solid two-phase flow first forms a high-velocity flow under the throttling effect of the valve spool and enters into the valve chamber, then the high-velocity flow develops sufficiently inside the valve chamber, and finally the gas flow and a part of the particles enter into the downstream pipe.

The prototype of the NTV in this article is JLK 65 × 30-35. The diameters of the upstream and downstream flow paths of the valve are 30 mm and 65 mm, respectively. The diameter of the spool is 38 mm. The cylindrical valve chamber is 92.5 mm high and 75 mm in diameter. For a fully developed particle and gas flow before entering the valve chamber and to avoid backflow, the upstream and downstream pipe lengths are greater than 20 times of the pipe diameter.

We postulate that the particles and the gas flow share identical velocities at the inlet boundary, with the assumption that particle fragmentation or coalescence does not occur during collision events. The diameters of the particles are 200, 300, 400, 500 and 600 μm, and the mass flow rate of the particles is constant at 0.904 g/s. The particle diameter and mass flow rate in this paper are determined by the previous experiments and the working conditions of the production site of the shale gas field in Chongqing, China. The physical travel length of the valve from fully open to fully closed is divided into four equal parts to obtain the openings 0, 0.25, 0.5, 0.75 and 1. When the valve is opened to 0, there is no airflow and no particles flow through the valve chamber, so this paper focuses on the four openings of 0.25, 0.5, 0.75 and 1. The specific physical properties of the gas flow, particles and geometry are shown in Table 1. Specific example parameter settings are shown in Table 2.

Table 1
Key parameters of the physical model.

	Unit	Gas stream	Particle	Geometry
Material		CH_4	Sand	Steel
Density (ρ)	kg/m^3	0.6679	2800	8030
Dynamic viscosity (ν)	Pa·s	1.087×10^{-5}		
Young's modulus (E)	GPa		50	196
Poisson's ratio (υ)			0.3	0.26

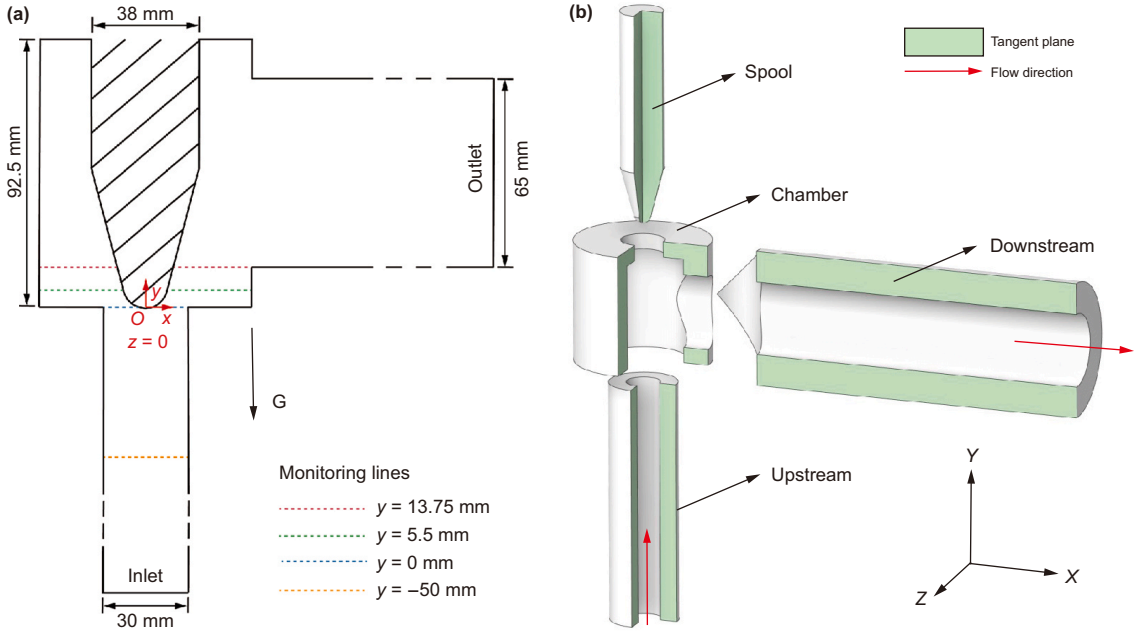

Fig. 1. **(a)** Valve dimension schematic diagram ($z = 0$ plane). **(b)** Valve 3D component decomposition diagram.

Table 2
Calculation parameter setting table.

Case	VOD	D_p, μm	u_{gas}, m/s
1	0.25, 0.5, 0.75, 1	0	30
2	0.25	200, 300, 400, 500, 600	30
3	0.5	200, 300, 400, 500, 600	30
4	0.75	200, 300, 400, 500, 600	30
5	1	200, 300, 400, 500, 600	30
6	0.25	400	20, 25, 35, 40
7	0.5	400	20, 25, 35, 40
8	0.75	400	20, 25, 35, 40
9	1	400	20, 25, 35, 40

3. Methodology

Combined with the content of Chapter 2, it can be found that NTV has a relatively complex internal structure, which is very easy to lead to particle aggregation and high-frequency impact on the wall. The CFD-DEM method is a "four-way coupling" model, which takes particle-particle, particle-gas flow, and particle-wall interaction forces into account. This method solves the particles based on Newton's second law, which can not only superimpose different contact models to give different characteristics to the particles, but also greatly improve the calculation accuracy in the case of high particle density. The biggest disadvantage of the DEM is that it requires more computational resources. This is because DEM uses an explicit method for calculations, which often require extremely small time insteps. However, with the improvement of computer hardware performance and parallel computing efficiency, the feasibility of using the discrete element method for computing has also been greatly improved. The CFD-DEM "four-way coupling" method has also become a very promising method in the field of gas-solid two-phase flow erosion.

The internal structure of the NTV in shale gas fields is relatively complex, and particles are prone to serious accumulation in the local area of the valve. To improve the calculation accuracy, a four-way coupling calculation model based on CFD-DEM method has been constructed. Fig. 2 is the flowchart of the CFD-DEM coupling method, where the CFD and the DEM solvers first establish the connection and initialize the coupling before the formal computation starts.

Due to the explicit time integration used in the DEM, multiple time steps are required to simulate the CFD single time step. During the calculation of DEM, the smaller the time step chosen in the simulation, the more stable the calculation will be, and the longer the simulation will take. However, if the time step chosen for the simulation is too large, the energy of the collision between the particles will increase relatively after the completion of a time step calculation, which may cause the particles to "explode" or pass through the geometry. After integrating the characteristics of the model, Rayleigh Time and other requirements, the time step in DEM is set to 5×10^{-8} s (the ratio of fixed time step to Rayleigh time step is less than 30%), and the time step in CFD is 10^{-4} s (each CFD calculation corresponds to 2000 steps in the DEM calculation node). Each case requires about 500 core-hours. When the coupling calculation starts, the gas flow field is first solved by the CFD calculation node and the results are transferred to the DEM calculation node through the coupling interface. After the force exerted by the gas flow field on the particles is obtained, the DEM starts to calculate the motion of the particles under the combined force and transfers the results of the particles through the coupling interface to the CFD calculation node. Fluent and EDEM are used for the above calculation process.

3.1. Gas phase model

The gas flow is a continuous phase, and there are two kinds of governing equations: Model A and B. The difference between the two models depends on the treatment of the pressure source term in the governing equation. In general, if the pressure is attributed to the fluid phase alone, it is called Model B. If the pressure is shared by the fluid and solid phase, it is called Model A (Zhou et al., 2010). The gas-solid two-phase flow can be regarded as a simplified version of Model A in this paper. The summary of Model A is as follows.

The equation for the conservation of mass in Eq. (1):

$$\frac{\partial(\varepsilon_g \rho)}{\partial t} + \nabla \cdot (\varepsilon_g \rho \mathbf{u}) = 0 \tag{1}$$

where ε_g is the porosity; ρ is the density; $\mathbf{u}$ is the time average velocity of the fluid.

The law of conservation of momentum is actually Newton's second law and can be expressed in Eq. (2):

$$\frac{\partial}{\partial t}(\varepsilon_g \rho \mathbf{u}) + \nabla \cdot (\varepsilon_g \rho \mathbf{u}\mathbf{u}) = -\varepsilon_g \nabla p + \varepsilon_g \nabla \cdot \boldsymbol{\tau} + \varepsilon_g \rho \mathbf{g} - \mathbf{F}_{pf}^{\mathrm{Set}\|} \tag{2}$$

where p is the static pressure; $\rho\mathbf{g}$ is the gravitational body force; $\mathbf{F}_{pf}^{\mathrm{Set}\|} = \frac{1}{\triangle V}\sum_{i=1}^{n}\left(\mathbf{f}_{\mathrm{d},i} + \mathbf{f}_i''\right)$ and $\mathbf{f}_{pf,i} = \mathbf{f}_{\mathrm{d},i} + \mathbf{f}_{\triangle p,i} + \mathbf{f}_{\triangle \tau,i} + \mathbf{f}''$

When talk about turbulence model, the near wall damping function in the $k-\varepsilon$ model is unreliable in a variety of flows and the traditional $k-\omega$ model is sensitive to the freestream value of ω that is applied at the inlet and outlet boundary (Menter, 1994). The $k-\omega$ SST (Shear-stress transport model) can address these problems and draw a more precise separation flow near wall. At this work, the $k-\omega$ SST model has been used to solve the turbulence.

3.2. Particle motion model

3.2.1. The discrete phase

In CFD-DEM, the coupling between particle-scale DEM and calculated unit-scale CFD must be considered. In this work, the trajectories of discrete phase particles are predicted by integrating the integrated external forces exerted by particles on particles. The equation of motion for particle shows in Eq. (3):

$$m_i \frac{\mathrm{d}\boldsymbol{u}_i}{\mathrm{d}t} = \mathbf{f}_{pf,i} + \sum_{j=1}^{k_c}\left(\mathbf{f}_{\mathrm{c},ij} + \mathbf{f}_{\mathrm{d},ij}\right) + m_i \mathbf{g} \tag{3}$$

where $\mathbf{u}_i$ is the translational velocitie of the particle, k_c is the number of particles interacting, $\mathbf{f}_{pf,i}$ is the particle-fluid interaction force and it can be expressed as $\mathbf{f}_{pf,i} = \mathbf{f}_{\mathrm{d},i} + \mathbf{f}_{\triangle p,i} + \mathbf{f}_{\triangle \tau,i} + \mathbf{f}''$, $\mathbf{f}_{\mathrm{c},ij}$ and $\mathbf{f}_{\mathrm{d},ij}$ are the elastic and viscous damping forces between particles, respectively.

The τ_r is the relaxation time of the particle calculated by Eq. (4):

$$\tau_r = \frac{\rho_p D_p^2}{18\mu}\frac{24}{C_d \mathrm{Re}} \tag{4}$$

where τ_r is the time constant of the exponential decay of the particle velocity caused by the drag force. Here, μ is the molecular viscosity of the fluid, D_p is the particle diameter, C_d is the drag coefficient and Re is the relative Reynolds number (Gosman and Loannides, 1983). The equation of C_d shows in Eq. (5) and equation of Re shows in Eq. (6).

$$C_d = a_1 + \frac{a_2}{\mathrm{Re}} + \frac{a_3}{\mathrm{Re}^2} \tag{5}$$

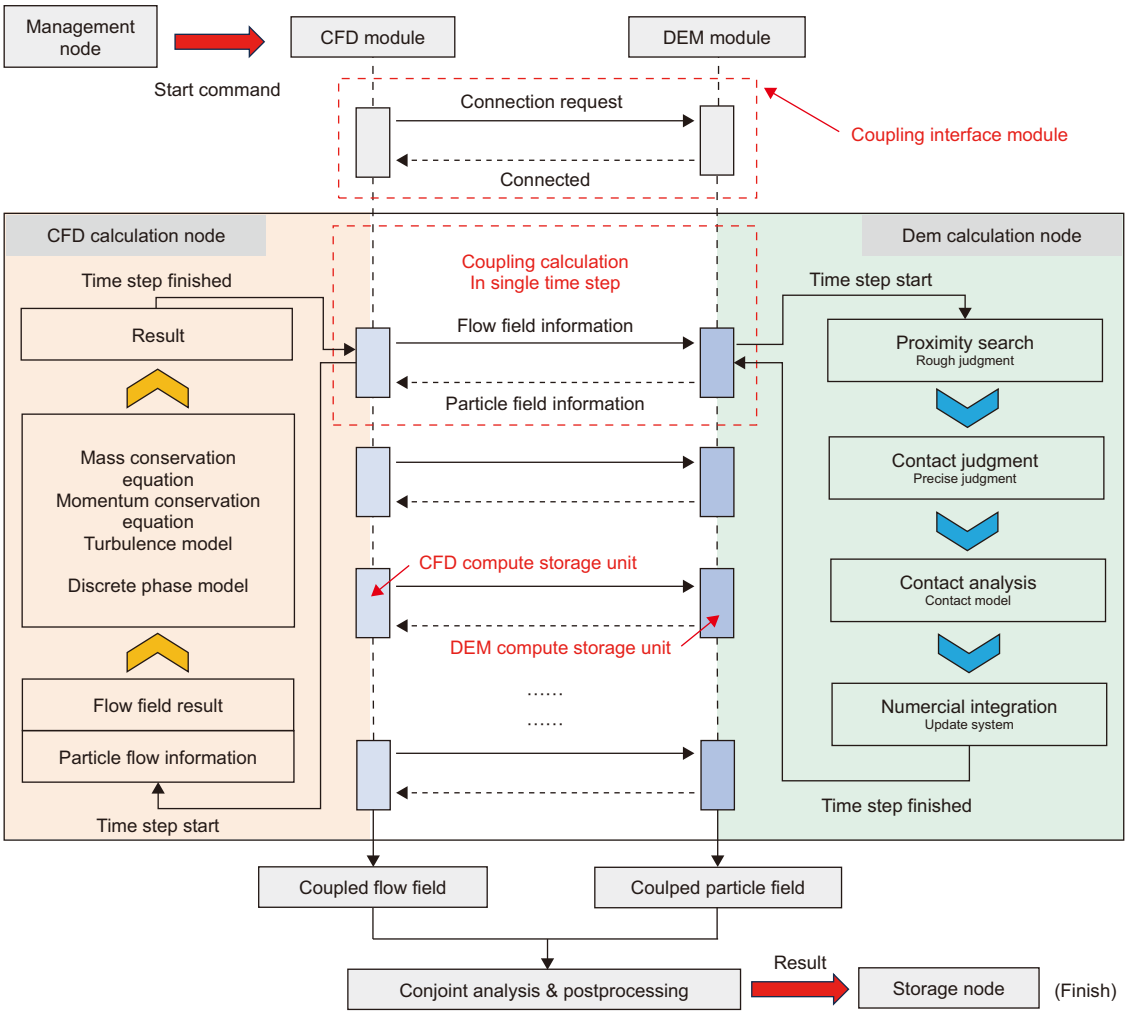

Fig. 2. CFD-DEM coupling calculation flow chart.

where a_1, a_2 and a_3 are constants that apply over several ranges of Re given by Morsi and Alexander (Morsi and Alexander, 1972).

The relative Reynolds number Re can be determined by the following equation.

$$\mathrm{Re} = \frac{\rho D_\mathrm{p} |\boldsymbol{u}_\mathrm{p} - \boldsymbol{u}|}{\mu} \tag{6}$$

where μ is the molecular viscosity of the fluid, D_p is the particle diameter. The u and ρ are the flow velocity and density of gas phase, respectively. The u_p is the velocity of solid particles.

The drag force can be expressed as $F_\mathrm{drag} = m_\mathrm{p}\frac{u-u_\mathrm{p}}{\tau_r}$. By bringing Eq. (6) of Re into formula equation (4) of τ_r. It can get the final form of drag force F_drag, writing it as an equation related to D_p and $u - u_\mathrm{p}$ for subsequent study in Eq. (7):

$$F_\mathrm{drag} = \frac{1}{8}\pi D_\mathrm{p}^2 \rho (u - u_\mathrm{p})^2 C_\mathrm{d} \tag{7}$$

where the F_drag is the drag force of gas flow on particle.

Due to the variable flow channels in NTV, the interaction force between particles and gas flow is very complex, the D_p is correlated with the effect of the gas flow on the particles, and this correlation is quantified here using the Stokes number (Stk) in Eq. (8):

$$Stk = \frac{\tau_r u_0}{l_0} \tag{8}$$

where u_0 is the velocity of the gas flow away from the obstacle, and l_0 is the characteristic dimension of the obstacle Willert et al. (2018) (typically its diameter) or a characteristic length scale in the flow (like boundary layer thickness) (Raffel et al., 2018). When the particle diameter is small, the τ_r of the particle is also small, which in turn leads to a low value in the Stk of the particle. When the particle has a small Stk, it is easier to follow the streamlines of the gas flow to achieve "perfect advection", while when the D_p is larger, its Stk is also larger, and inertia and gravity will dominate its trajectory more.

3.2.2. The particle contact model

The CFD-DEM model takes the interaction forces between particles into account. This can better solve the collision problem between particles caused by high particle density. The main forces in the contact model contain the normal force F_n, the tangential force F_t and their corresponding damping force F_n^d and F_t^d. In addition, the model is also suitable for contact collisions between particles-wall, where the wall is treated as spherical particle with infinite radius. Fig. 3 is the illustrative

diagram of the particle contact model. Fig. 3(a) is a schematic diagram of the particle-particle contact, Fig. 3(b) is a schematic diagram of the particle-wall contact, and Fig. 3(c) is the contact force model.

The normal force F_n is a function of normal overlap δ_n and be defined in Eq. (9):

$$F_n = \frac{4}{3}E^*\sqrt{R^*}\delta_n^{\frac{3}{2}} \tag{9}$$

where the E^* and R^* are the equivalent Young's Modulus and radius, respectively.

In addition, there is a normal damping force, F_n^d, given by Eq. (10):

$$F_n^d = -2\sqrt{\frac{5}{6}}\frac{-\ln e}{\sqrt{\ln^2 e+\pi^2}}\sqrt{S_n m^*}\mathbf{v}_n^{rel} \tag{10}$$

where m^* is the equivalent mass, e is the coefficient of restitution, $\mathbf{v}_n^{rel}$ is the normal component of the relative velocity, S_n is the normal stiffness and be defined in Eq. (11):

$$S_n = 2E^*\sqrt{R^*\delta_n} \tag{11}$$

The tangential force F_t is defined in Eq. (12):

$$F_t = -S_t\delta_t \tag{12}$$

where δ_t is the tangential overlap, S_t is the tangential stiffness and be defined in Eq. (13):

$$S_t = 8G^*\sqrt{R^*\delta_n} \tag{13}$$

were G^* is the equivalent shear modulus.

Additionally, tangential damping F_t^d is given by Eq. (14):

$$F_t^d = -2\sqrt{\frac{5}{6}}\frac{-\ln e}{\sqrt{\ln^2 e+\pi^2}}\sqrt{S_t m^*}\mathbf{v}_t^{rel} \tag{14}$$

where $\mathbf{v}_t^{rel}$ is the relative tangential velocity.

This paper, as well as most DEM models, employ simplified particle collision models such as the soft ball model (simulating contact with a spring-damping system) or the hard ball model (instantaneous contact). Although these models perform well at the macroscopic level, they cannot accurately capture the microscopic contact behavior of particles at high strain rates or complex shapes, especially in inelastic or adherent particle systems. In the future, we will carry out experiments and simulation calculations of particles of different shapes to improve the accuracy of particle erosion.

3.3. Particle erosion model

At this work, the erosion rate (ER) of valve components is calculated by the Oka erosion model proposed by Oka and Yoshida (Oka et al., 2005; Oka and Yoshida, 2005) in Eq. (15). Compared with other erosion models, the Oka erosion model has the most advantages in comprehensively considering the properties of solid particles (velocity, mass, diameter) and the erosion surface (density, hardness, curvature) of the valve. The use of Oka erosion model can fully consider the physical properties of particles and the characteristics of the inner wall surface of the valve. In this model, there are only two input parameters (H_v, W) are required.

$$ED = 65W^{-k}\left(\frac{V}{V_{ref}}\right)^{2.3H_v^{0.038}}\left(\frac{D}{D_{ref}}\right)^{k_1}\frac{m_p}{A}f(\alpha) \tag{15}$$

where ED is the erosion depth, W is the materials wear constant, k is the experimentally derived coefficient, V is the particle impact velocity, V_{ref} is the reference velocity, H_v is the Vicker's hardness, D is the particle diameter, D_{ref} is the particle reference diameter, m_p is the particle mass, A is the particle projection area, $f(\alpha)$ is the impact angle function and be defined in Eq. (16). The values of the parameters are shown in Table .3.

The impact angle function is determined as:

$$f(\alpha) = (\sin\alpha)^{0.71H_v^{0.14}}(1+H_v(1-\sin\alpha))^{2.4H_v^{-0.94}} \tag{16}$$

where α ($\alpha \le 90^\circ$) is the particle impact angle.

4. Validation

4.1. Mesh independence validation

In numerical calculations of erosion, the physical model is cut into many meshes of smaller size. Due to the presence of the mesh, there is a discrete error between the computed value and the accurate value, which decreases as the mesh density increases. However, a finer mesh means that more computational resources or longer computation time is required (Cloete et al., 2015; Cloete et al., 2016; Wu et al., 2024). As shown in Table 4 and Table 5, the number of meshes of the model is divided into different levels (M1–M4). Different levels of mesh correspond to different meshing methods and mesh quality. All levels of mesh met the mesh quality requirements needed for the calculation.

To more accurately resolve the flow field adjacent to the boundary layer and enhance the computational precision of the contact model, the turbulence model used in this paper is $k-\omega$ SST. It requires the value of y^+ close to 1. In this paper, the value of the y^+ is controlled by controlling the size of the first boundary layer of the wall. In practical problems, it is extremely difficult to control the values of y^+ in all positions around 1. Since the study in this paper focuses on large-scale eddy structures, in this case, the value of $y^+ < 2$ can maintain a reasonable amount of computation while ensuring the calculation accuracy. The first layer of the mesh is all located within the viscous sublayer with $y^+ < 2$. As shown in Fig. 4, the values of the y^+ under the four VODs are within the range set in this paper.

In addition, the meshes near the spool where the flow field changes violently are refined locally, and the meshing details are shown in Fig. 5. The mesh independence validation is carried out using a particle size of 400 μm, an inlet flow velocity of 30 m/s, and a valve opening degree of 0.25. The calculation results are shown in Fig. 6, when the number of meshes reaches M3 level, the average error of both the maximum spool erosion rate and the chamber deposition rate is less than 2% compared with the results obtained with the M4 level mesh. This indicates that when the mesh count reaches 788,499, further mesh refinement to improve computational accuracy is no longer justified. In contrast, the M3 mesh achieves the required numerical precision while maintaining significantly lower computational time (see Fig. 7).

This indicates that when the number of meshes reaches 788,499, it is not meaningful to increase the number of meshes to improve the accuracy of the calculation results, and the M3 mesh can complete the calculation with less kernel time while meeting the calculation accuracy. Therefore, this paper chooses to use the M3 level mesh for the subsequent calculations.

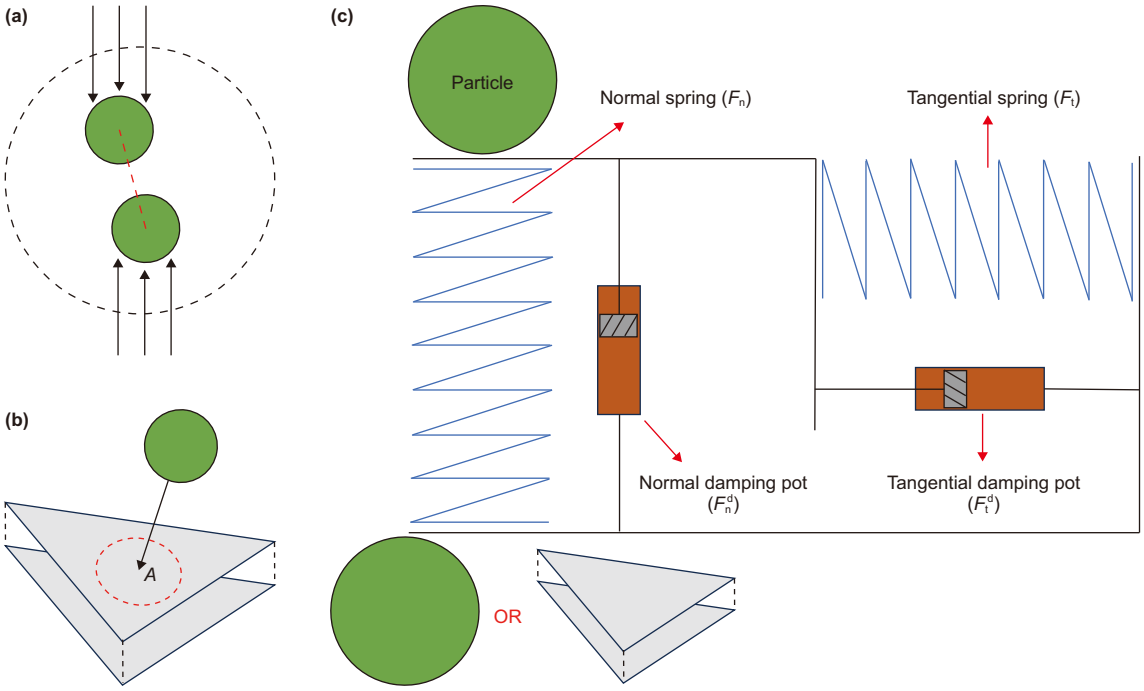

Fig. 3. Particle contact model. **(a)** Schematic of particle-particle contact. **(b)** Schematic of particle-wall. **(c)** Contact force model.

Table 3
Erosion model constant.

Constant	Unit	Value
W		10
H_v	GPa	1.77
V_{ref}	m/s	104
D_{ref}	μm	326
k_1		0.19

Table 5
Mesh quality parameters.

Mesh level	Average skewness	Minimum orthogonality quality	Maximum aspect ratio
M1	0.32	0.31	55.2
M2	0.19	0.37	35.0
M3	0.16	0.4	30.7
M4	0.15	0.41	28.3

4.2. Flow erosion accuracy validation

In order to ensure the accuracy of the computation, two studies are used to validate the CFD-DEM coupling computational model in this paper. The first is the multi-angle circular column erosion simulation and experimental results previously completed by our team (Hong et al., 2023), where the velocity of the gas flow and the particles are 28.82 m/s, the particle mass flow rate is 11.37 g/s. In this model, high-velocity particles are horizontally ejected from the nozzle and impact the specimen, and the angle of impact of the particles on the specimen can be changed by rotating the specimen. The second is the throttle valve erosion simulation and experimental results by Zhu et al. (2014), where the inlet flow velocity is 30 m/s, the VOD is 0.75, the inlet diameter is 30 mm, the particle diameter is 200 μm, the particle concentration is 6%. In this model, solid particles enter the throttle valve from upstream and cause erosion to the throttle. The physical properties of the materials in the above cases are shown in Table 1.

The results indicate that, compared to the CFD-DPM approach, the CFD-DEM methodology exhibits a smaller average relative error between computational predictions and experimental measurements. The average relative error between the computational results of the CFD-DEM model and the experimental results of the multi-angle circular column erosion model is 4.1%, and the average relative error with the experimental results of the valve erosion is 4.35%. Considering the systematic and random errors caused by the measurement, material properties and other factors during the experiment, the accuracy of the calculation model used in this paper is reliable.

5. Result and discussion

This section transitions from the model setup to a rigorous analysis of the computational results. We first establish a theoretical baseline by characterizing the pure gas flow field.

Table 4
The number of mesh under different levels.

Mesh level	Boi mesh	Surface mesh	Volume mesh	Mesh quantity	Node quantity
M1	2.5	2.5/20	2.5/20	285,248	113,195
M2	2	2/16	2/16	433,199	197,431
M3	1.5	1.5/12	1.5/12	788,499	383,670
M4	1	1/8	1/8	1,524,259	856,382

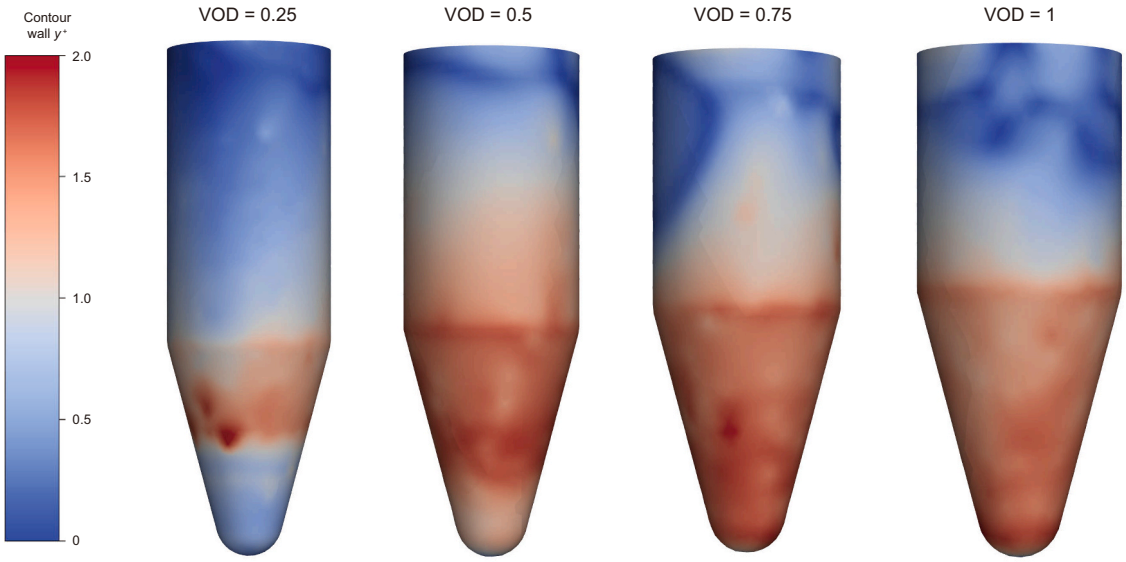

Fig. 4. The value of y^+ under the four VODs (the particle diameter $D = 400$ μm).

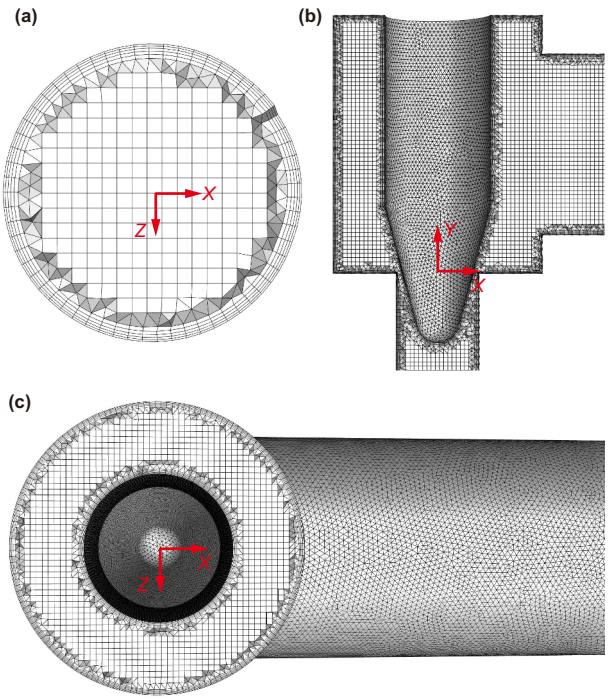

Fig. 5. Meshing (VOD = 0.25). **(a)** Cross-section of upstream pipeline. **(b)** Vertical section of Spool & Chamber. **(c)** Horizontal section of the upper part of the chamber.

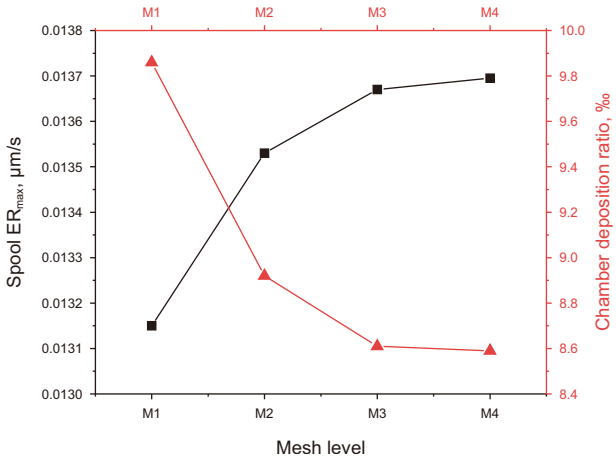

Fig. 6. Mesh independence validation.

Subsequently, the complex interplay between the valve opening degree (VOD) and particle diameter on the two-phase flow dynamics is analyzed, setting the stage for the final discussion on erosion mechanisms. The parameter settings for the cases discussed are detailed in Table 2.

5.1. Gas flow field

5.1.1. The effect of the VOD on the gas flow field

The change in the VOD directly changes the effective cross-sectional area of the runner, thereby controlling the local flow rate and turbulence intensity of the fluid. When the VOD is small, the fluid is highly compressed, creating a high-speed jet at the valve outlet, which significantly increases the velocity of the particles and causes strong local turbulence. As the VOD increases, the jet effect weakens, the velocity of the fluid field becomes more dispersed, and the turbulence intensity may also change.

Firstly, the pure gas flow field is studied, where there are no particles in the flow field. Gas flow phase is solved only by the CFD calculation node.

As shown in Fig. 8., in the process of gas flow from the upstream pipeline through the valve chamber into the downstream pipeline, it first contacts with the valve spool and forms a “low velocity zone” at the apex of the spool. Subsequently, the gas flow is accelerated in the process of passing through the throttling channel and as the valve opening decreases, the throttling effect of the needle valve is gradually strengthened, and the maximum value of the velocity in the flow field is gradually increased.

Influenced by the downstream pipeline, there is a large difference in the flow field between the left and right chambers of the valve chamber when the gas flow from the upstream piping passes

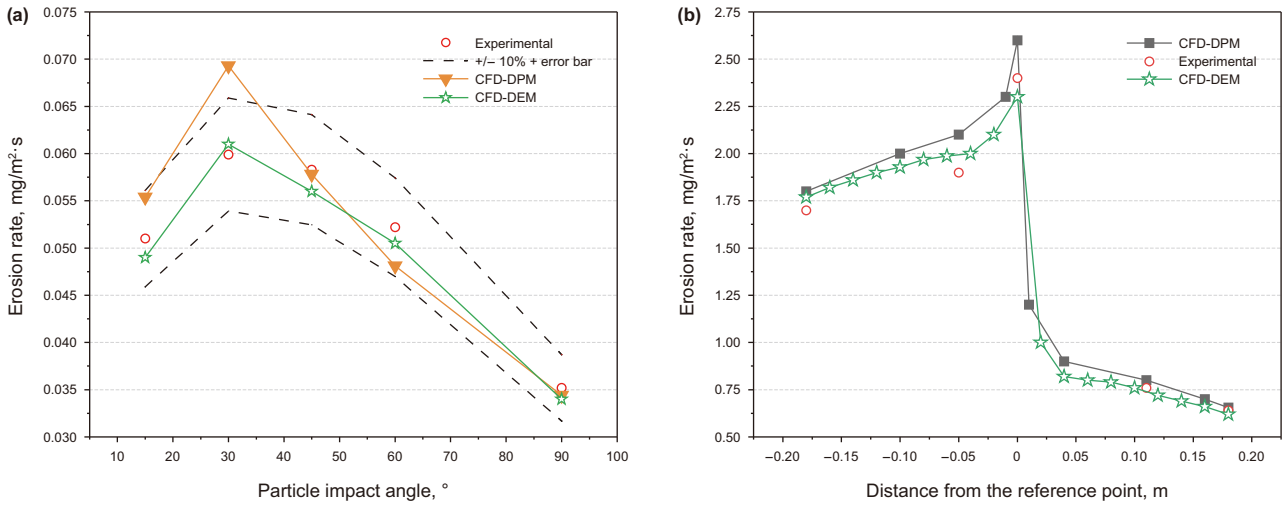

Fig. 7. Comparison of CFD and Experimental results. **(a)** Multi-angle circular column erosion model. **(b)** Throttle valve erosion model.

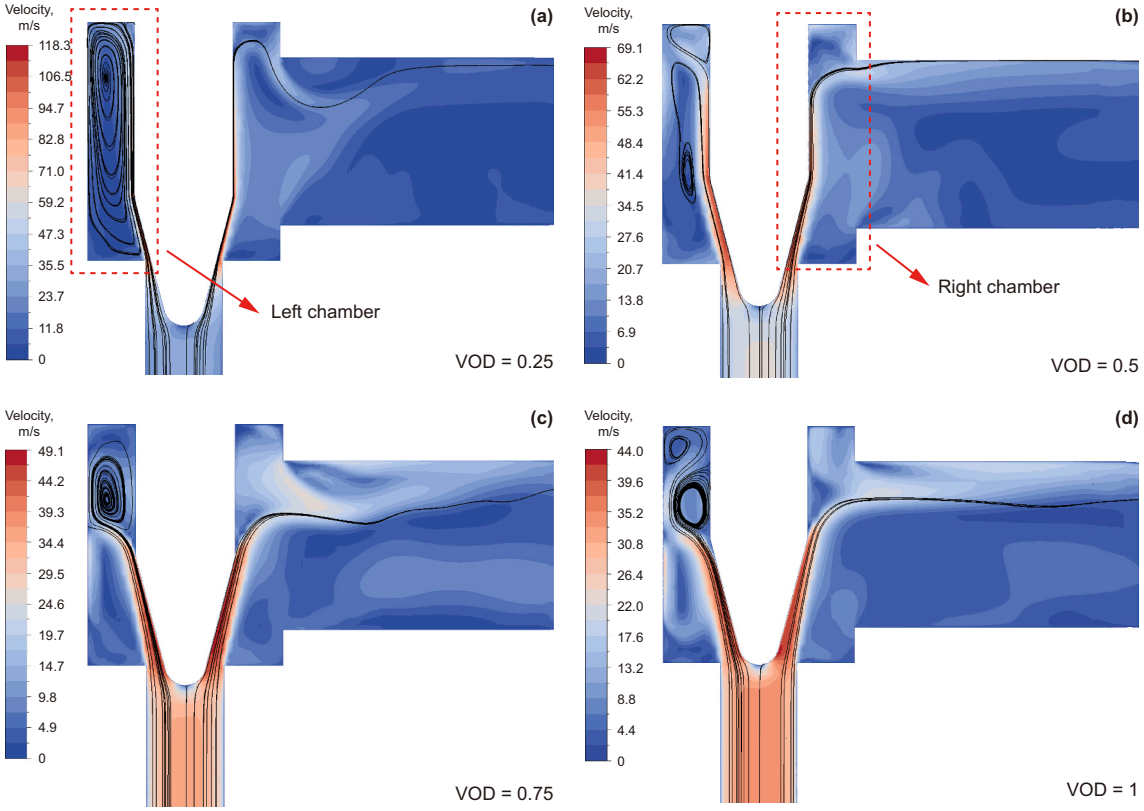

Fig. 8. Gas flow field under different valve opening degree.

through the throttling flow path. In the left chamber of the valve, the gas flow formed an obvious vortex in the restricted space, and the smaller the VOD, the larger the range of the vortex. It is worth noting that the vortex in the left chamber is separated when the VOD is 0.5 & 1. The main vortex has a larger range at the bottom of the chamber and the secondary vortex has a smaller range at the top of the chamber, and the two vortexes are in opposite directions. The difference is that when VOD = 1 the secondary vortex is close to the upper left wall while when VOD = 0.5 the secondary vortex is close to the upper right wall. However, when the VOD is 0.25 & 0.75, there is only one vortex in the left chamber of the valve chamber and no reverse vortex. In the right chamber, on the other hand, the gas first flows close to the wall of the spool under the effect of inertia. When the gas reaches the cylindrical wall of the spool it gradually begins to separate from the wall and flow toward downstream. The difference is that the smaller the VOD, the later the separation (the closer to the upper wall of the valve chamber).

5.1.2. *The effect of particle on the gas flow field*

With the addition of particles, the flow field inside the valve is gas-solid two-phase flow. The CFD and DEM calculation nodes are coupled to calculate the motion of the gas flow and particles, and the coupled calculation process is shown in Fig. 2.

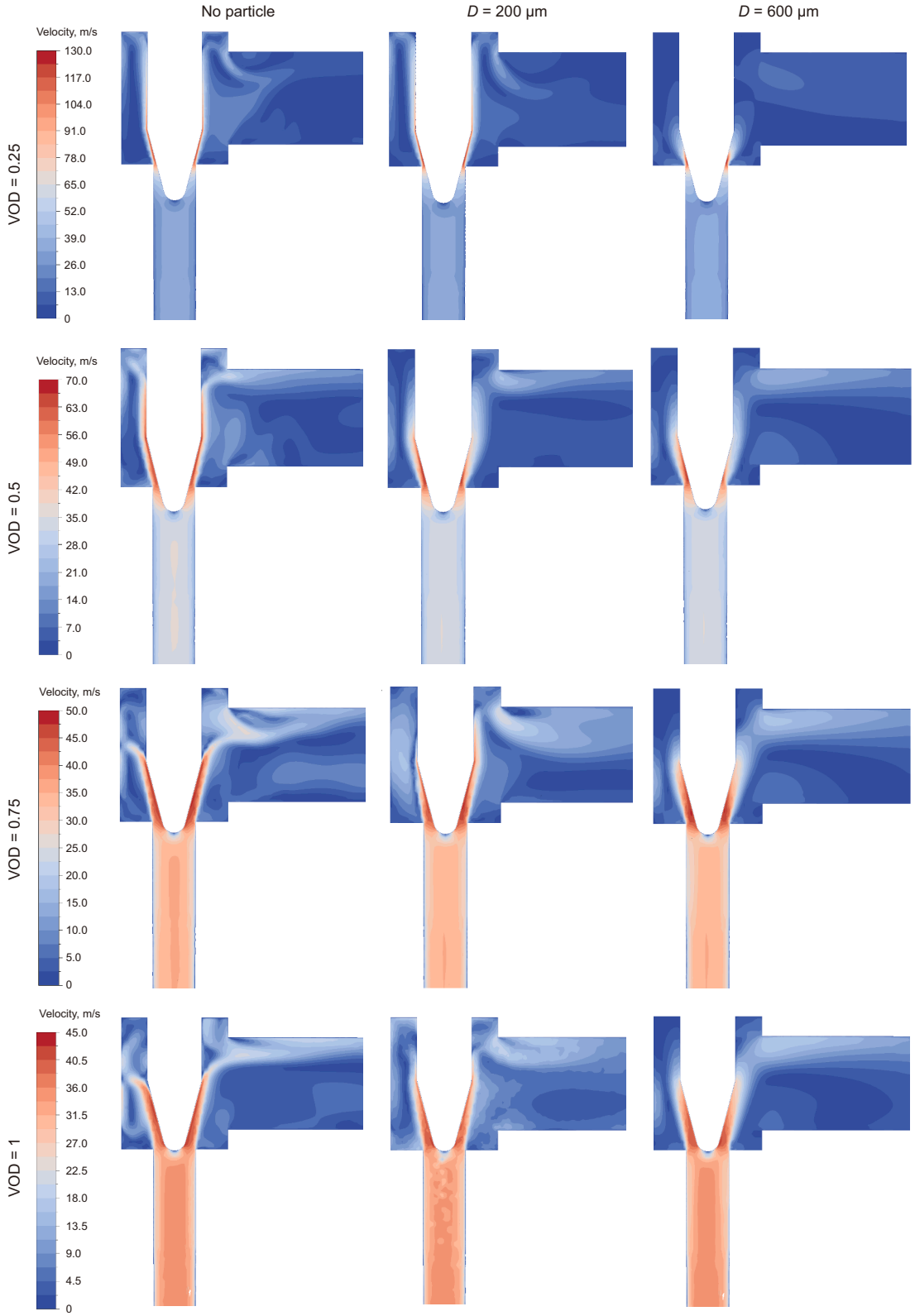

Fig. 9. Effect of particle on the gas flow field.

Fig. 9 shows the velocity field contour for different VOD without particles and with particle diameters of 200 and 600 μm, respectively, in cases 2–5. Before entering the valve chamber, the gas flow first contacts the valve spool and forms a stagnation zone at the top of the spool. Due to the different throttling effects of the valve at different VODs, the extreme value of the velocity in the flow field increases as the valve opening decreases.

Under the same VOD, with the increase of the particle diameter, the high-speed region of the gas flow field gradually shrinks toward the throttling channel, and this phenomenon becomes more and more obvious with the decrease of the VOD. The effect of particle diameter on the flow field is mainly localized due to the small percentage of volume actually occupied by the particles in the gas-solid two-phase flow.

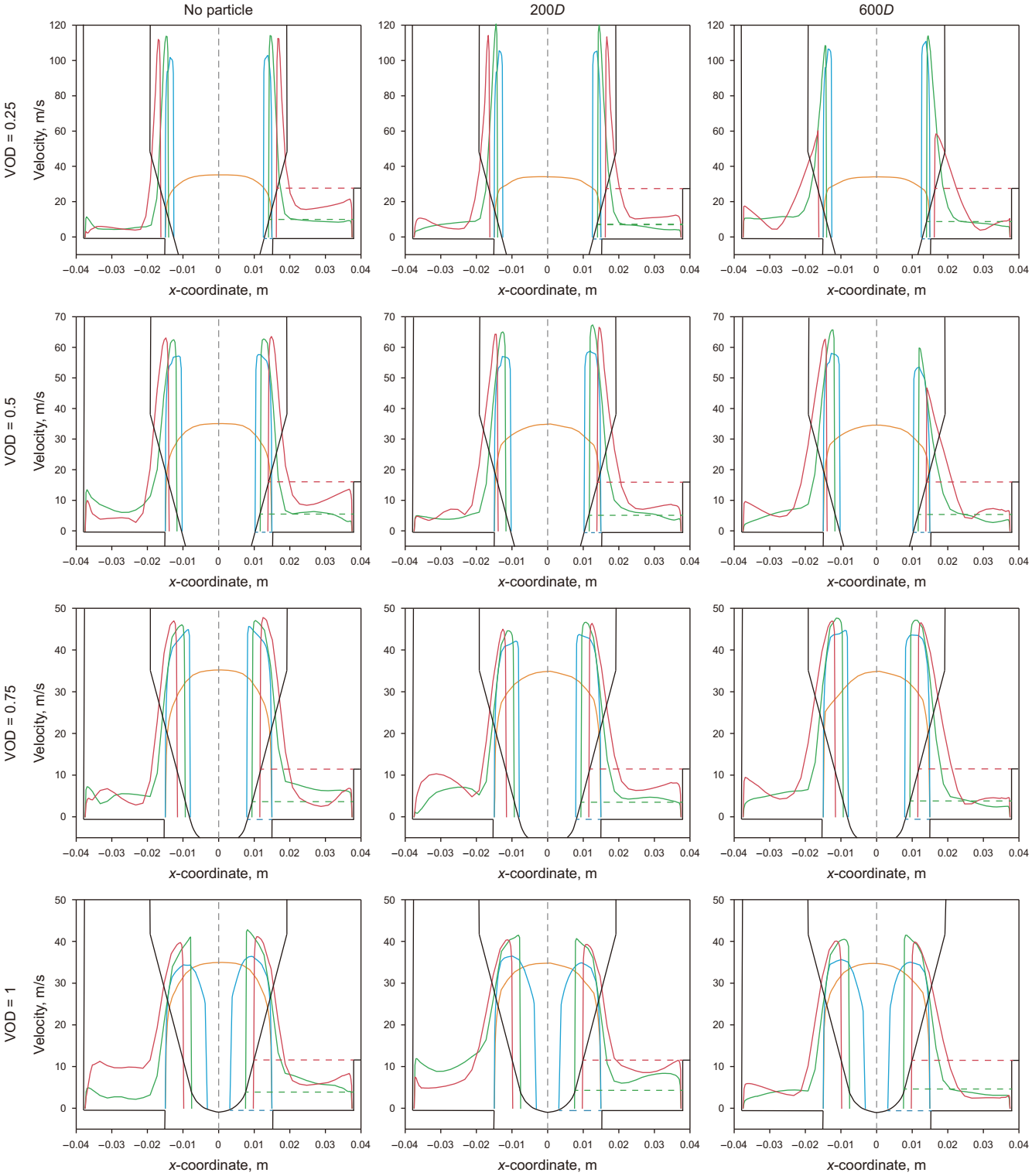

Fig. 10. Velocity at the monitoring line under different VOD and particle diameter.

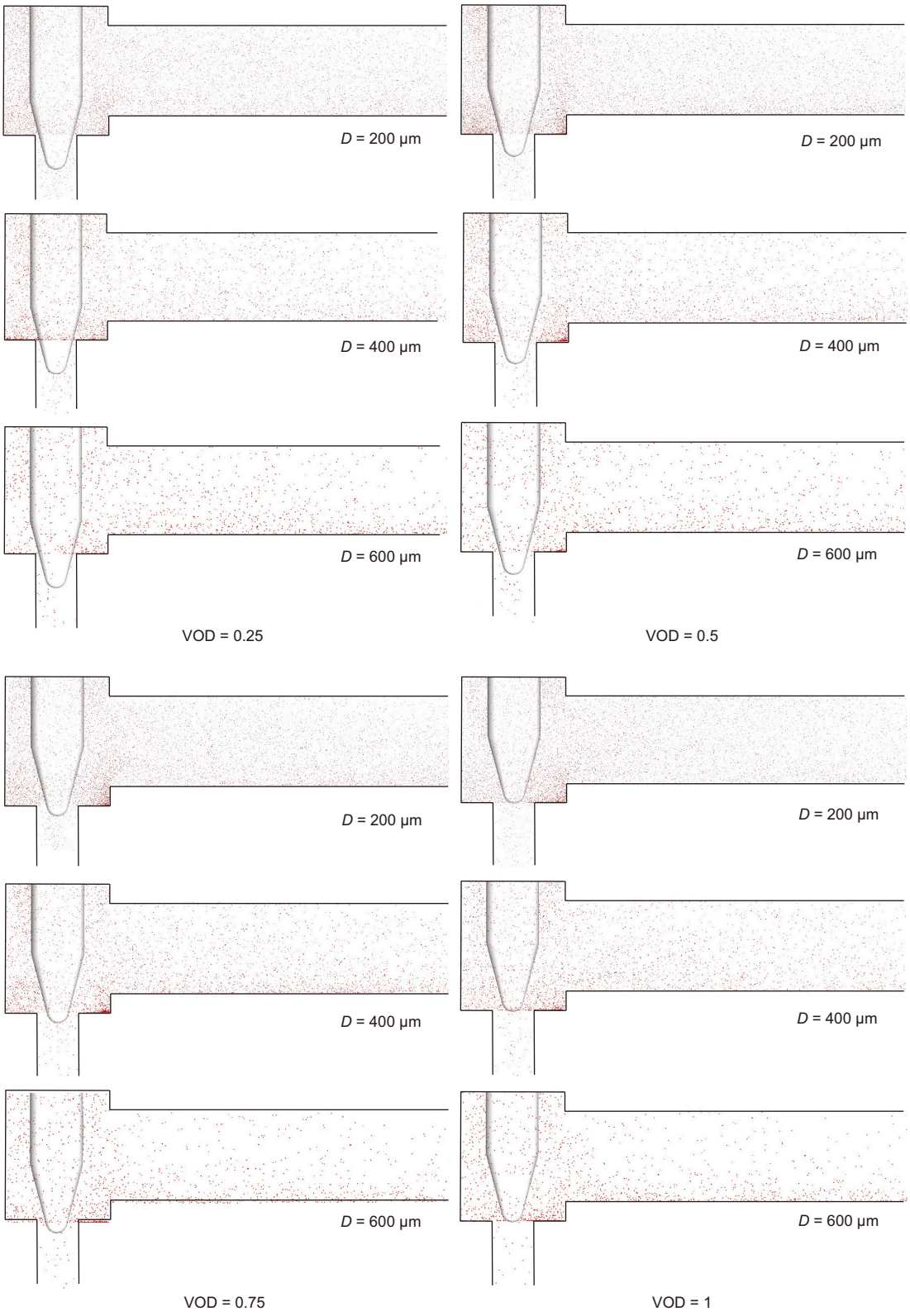

Fig. 11. Particle distribution under different VOD and particle diameters.

The velocity of the gas flow has a very strong influence on the motion of the particles. In order to quantitatively describe the velocity field, four horizontal velocity monitoring lines are set up in the *XY* plane at $Z = 0$. The positions of the monitoring lines are shown in Fig. 1 (a). The color of the curve in Fig. 10 is the same as the monitoring lines at the corresponding positions. Combined with Figs. 9 and 10, the influence of particles and valve opening degree on the flow field can be investigated qualitatively and quantitatively, respectively.

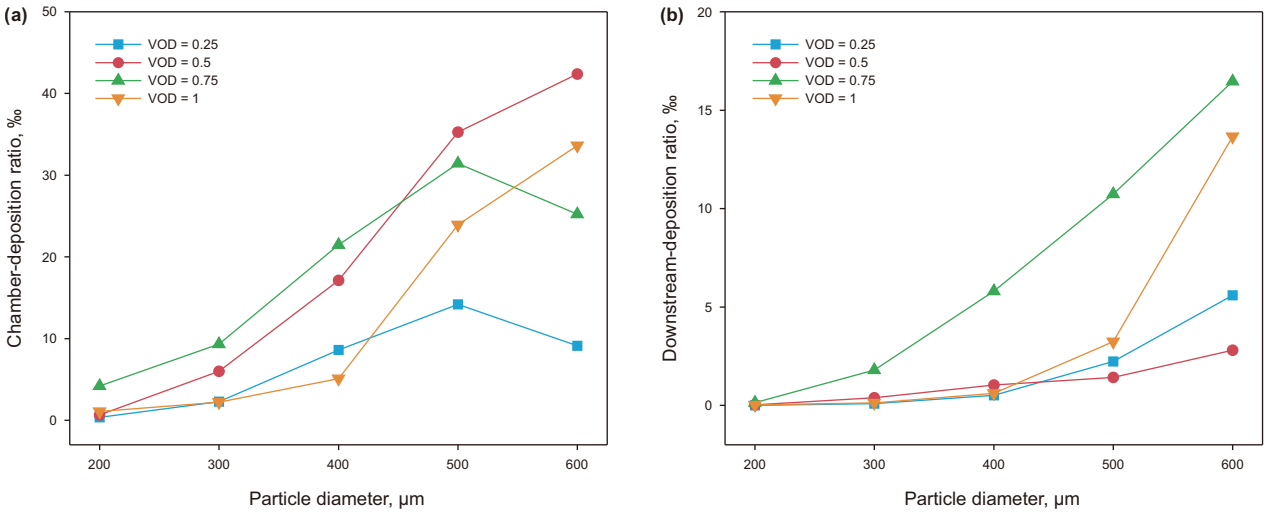

Fig. 12. Particle deposition rate under different VOD: **(a)** chamber, **(b)** downstream.

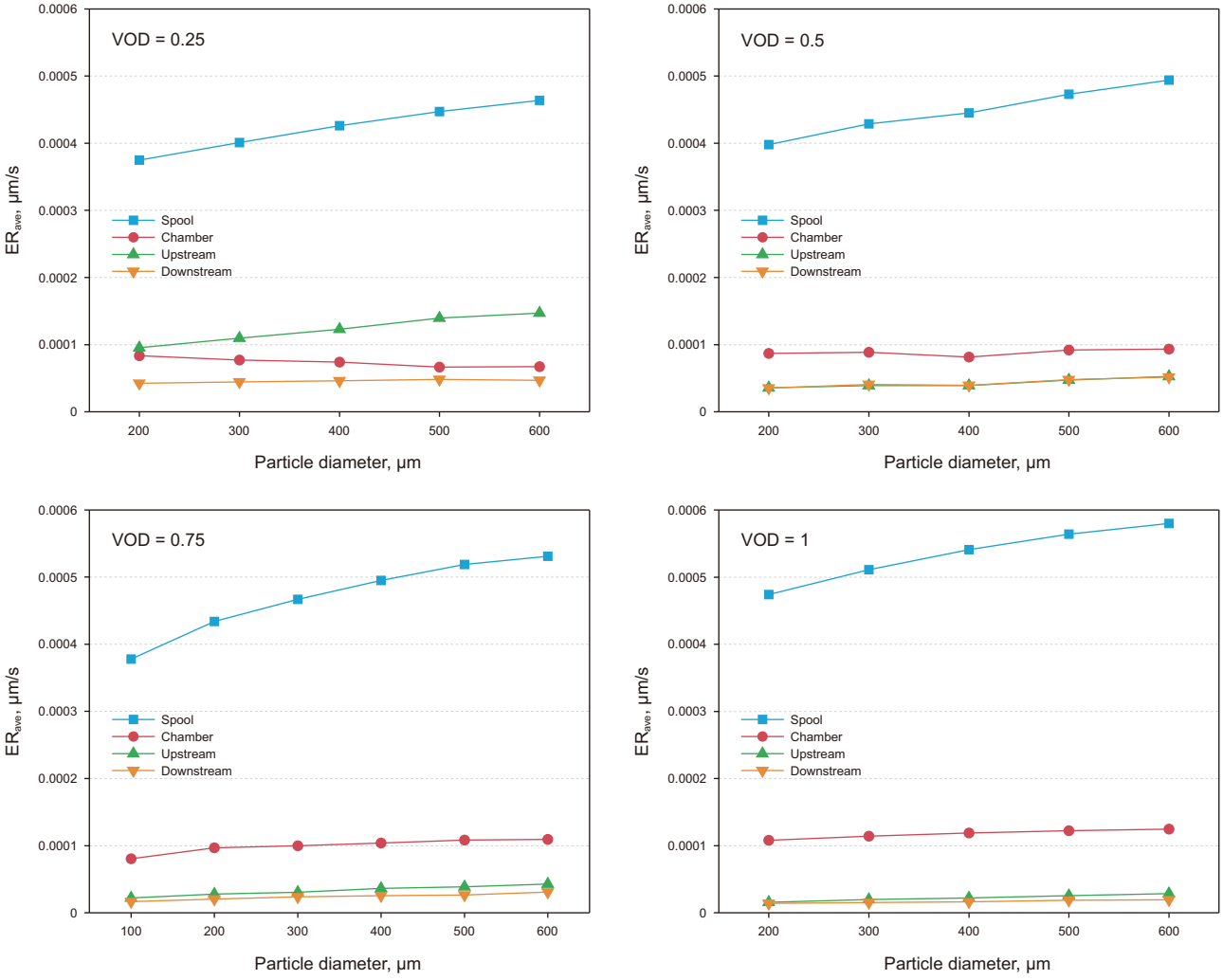

Fig. 13. Average erosion rate at different valve components.

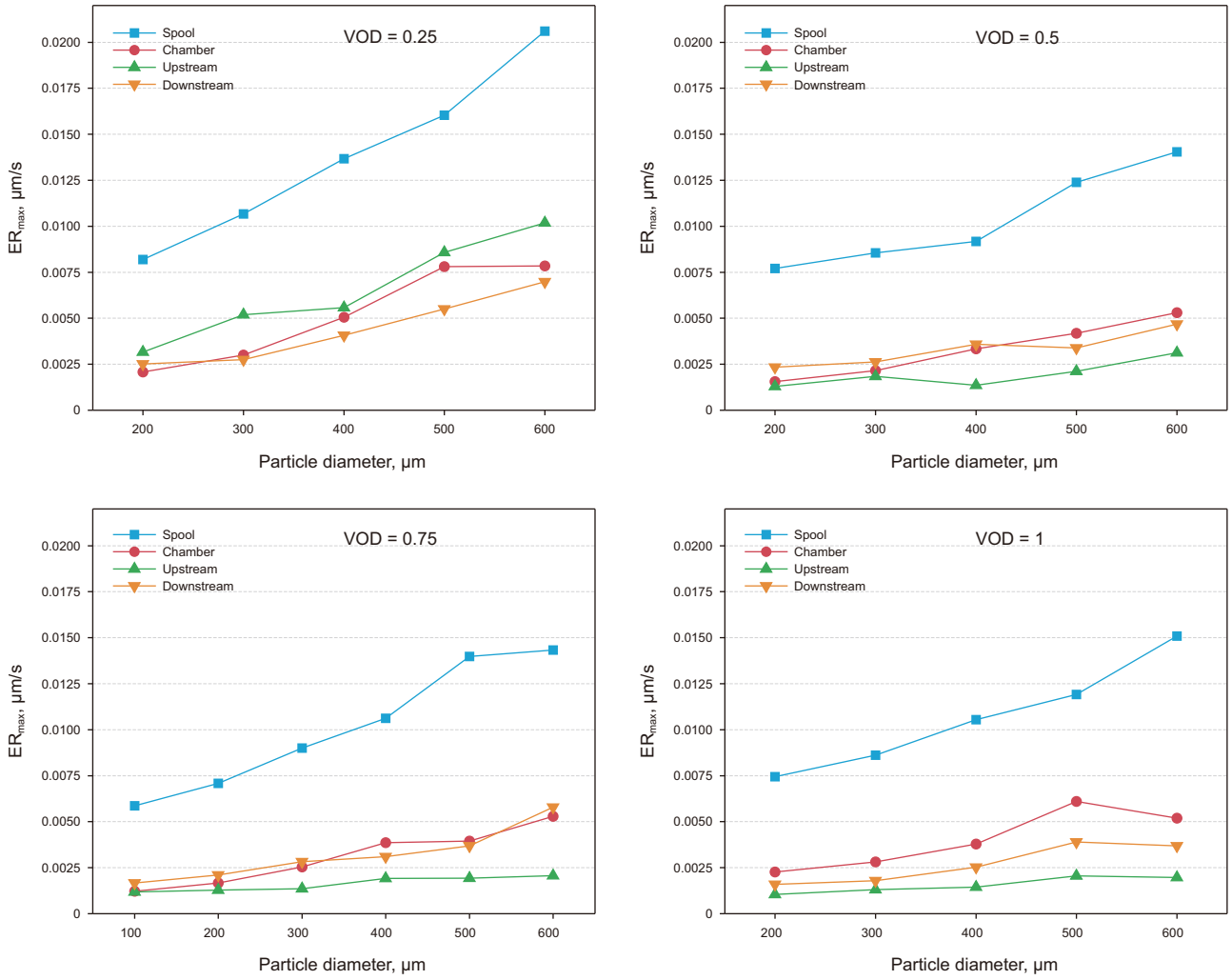

Fig. 14. Maximum erosion rate of different valve components.

The orange curve represents the velocity distribution at the $Y = -50$ mm position of the upstream pipeline. The change trend of this curve is relatively stable under any working conditions, which reflects that the flow field in the upstream pipeline is less affected by the VOD and particle diameter. The velocity change of the flow field from the center of the pipeline to the pipe wall conforms to the law of Newton inner friction.

When VOD = 0.25, the velocity of $y = 5.5$ mm near the spool position increases obviously, which is due to the particle with diameter of 200 μm will aggravate the throttling effect of the valve. When the particle diameter increases to 600 μm, the maximum of the velocity at the position of the detection line adjacent to the throttling channel decrease slightly, but the maximum of the velocity at the position of the monitoring line $y = 13.75$ mm has a significant decrease.

This is because the mass flow rate of the particles at this work is a constant value, and the volume of the throttling channel occupied by the particles is almost the same under different working conditions. The velocity of the gas flow through the throttle channel increases significantly, and the drag force on the particles is strongly influenced by the diameter of the particles and the relative velocity of the particles.

From the expression of the drag force (Eq. (5)), it can be seen that the drag force value increases exponentially with the increase in particle diameter (D_p) and the relative velocity of the gas stream and the particles $(u - u_p)$. Since the particles and the gas flow enter the valve from the upstream with the same velocity, the value of $u - u_p$ is the largest at this VOD, and the value of F_{drag} increases exponentially when the particle size increases from 200 to 600 μm, and the work done by the gas flow on the particles is also greatly increased. According to the principle of energy conservation, the kinetic energy of the gas flow is transferred to the particles, which leads to a significant reduction of the gas flow velocity on the $y = 13.75$ mm monitoring line. As the increase of the VOD, the throttling effect decreases, the difference between the velocity of the gas flow and the particles decreases, and the kinetic energy transferred from the gas flow to the particles also decreases.

The NTV mainly controls the throttling effect by controlling the VOD, and the area of the flow channel of the valve is different under different VODs. In order to be able to efficiently control the flow rate of the valve, the NTV has a wide opening range and has a great influence on the gas flow field. Particles mainly affect the flow field through the interaction force with the gas flow and the encroachment on the fluid space. Although the diameter of the particle has a certain influence on the gas flow field, its influence on the gas flow field mainly occurs locally. It has less of an impact than VOD, which directly change the area of the throttle channel.

Overall, the smaller the VOD, the more obvious the encroachment effect of particles on the throttle channel, and the effect increases with the increase of particle diameter. When the VOD is

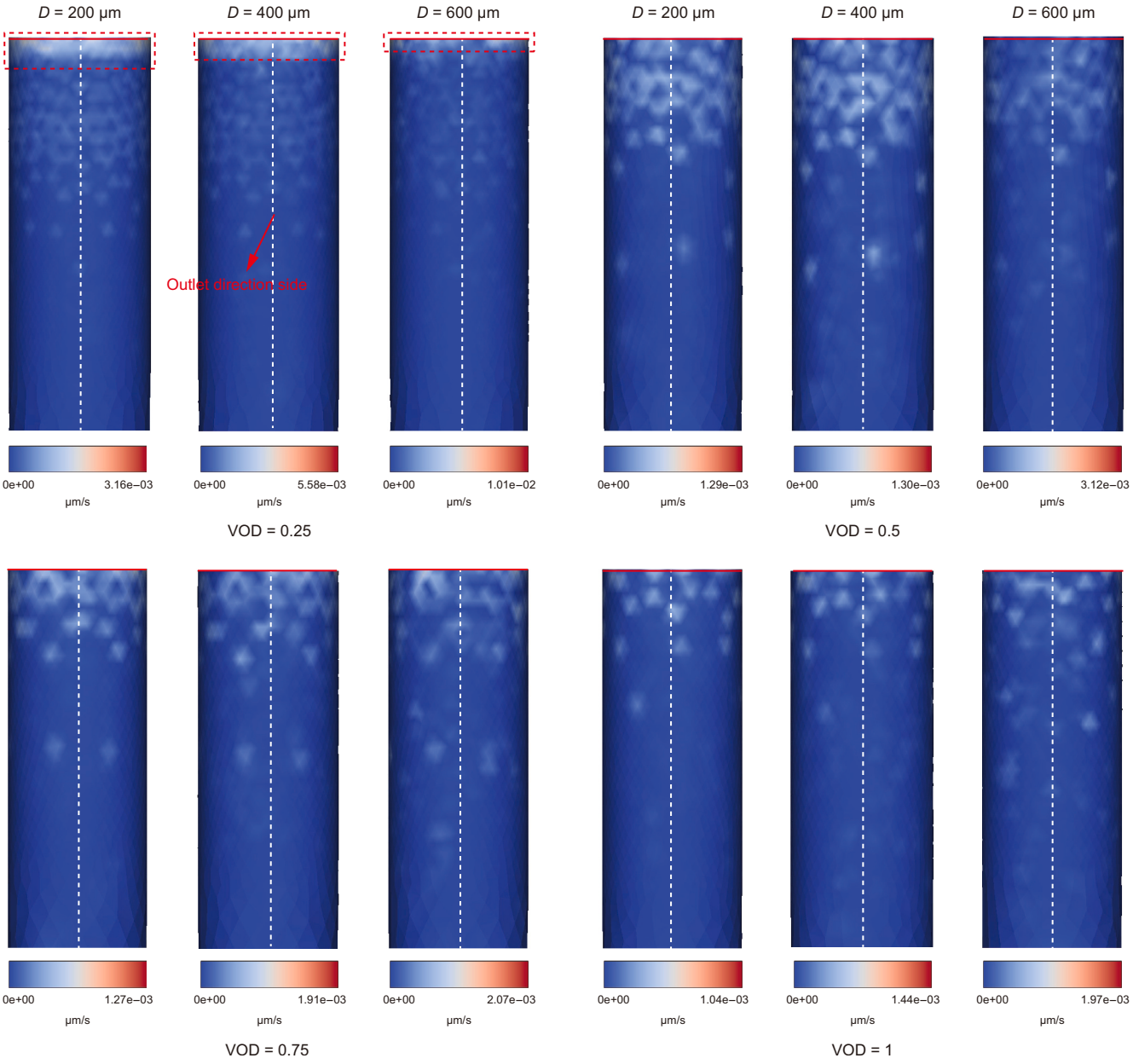

Fig. 15. Contour of upstream pipeline erosion rate distribution.

large, the effect of particle addition on the flow field is relatively slight, and the effect is mainly concentrated on the right side of the valve chamber near the wall.

5.2. Particle field

The main forces on the movement of particles in the flow field are inertia force, drag force, gravity and so on. Under the special structure of the NTV and the joint influence of the above combined forces, the particle diameter and VOD have a greater influence on the results of particle movement.

Fig. 11 shows the particle distribution in the flow field of the valve under different VOD and D_p. It is easy to find that the particle deposition is mainly concentrated on the right side of the chamber and the downstream. The distribution of particles in the flow channel becomes more and more uniform with the decrease of particle diameter under the same VOD. This phenomenon is most obvious in the downstream pipeline, which is least affected by the irregular shape of the valve interior. This is because the probability of head-on collision between the particles and the wall is greatly reduced and the vortex phenomenon is not obvious in this section of the pipe, so that gravity, drag force and inertial force almost dominate the motion of the particles. As the D_p increases, the *Stk* of the particles and the influence of gravity gradually increase, and the change of the particle deposition effect in the downstream pipe is most obvious (see Fig. 12).

In the chamber, the particle deposition rate increases with the increase of D_p when VOD = 0.5 & 1. However, the change in particle deposition rate is different when VOD = 0.25 & 0.75. The specific performance is as follows: With the increase of D_p, the particle deposition rate firstly increases gradually and reaches the peak value at D_p = 500 μm, and then the particle deposition rate

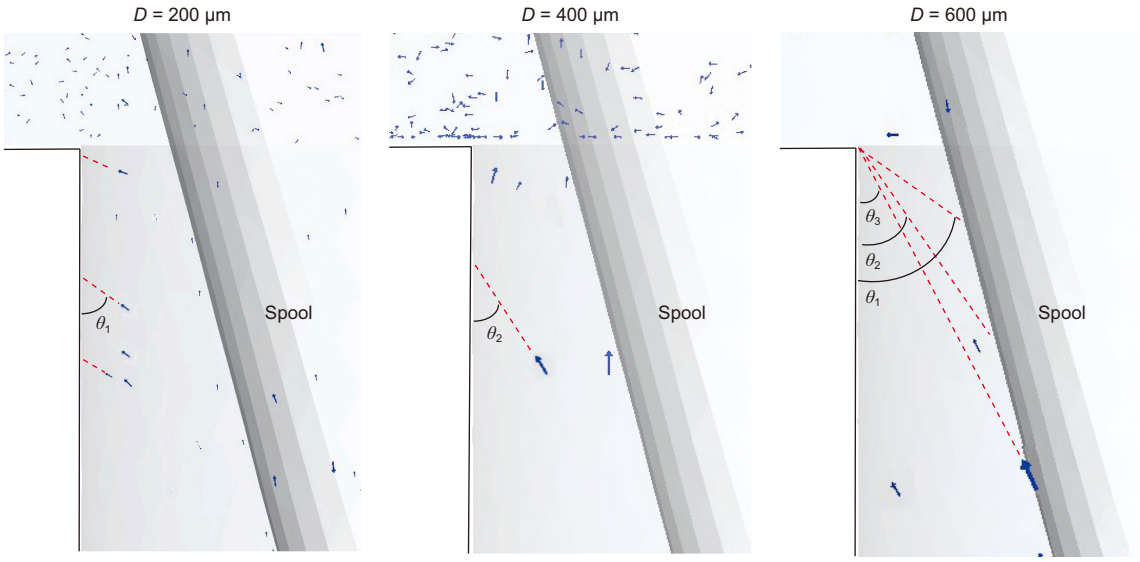

Fig. 16. Trajectory of particles after impacting the spool at VOD = 0.25.

decreases when the D_p increases to 600 μm. This indicates that when there is only a single vortex in the chamber, the particles have enough kinetic energy to escape from the chamber when the D_p increases to a certain value.

Meanwhile, the reverse vortices generated in the left chamber when VOD = 0.5 & 1 make the particle distribution, which is originally affected by the complex flow paths in the chamber, more chaotic. The chaotic particle distribution exacerbates particle-wall and particle-particle collisions in the chamber. These collisions greatly dissipate the kinetic energy of the particles. When the D_p is small, the particles are influenced by the drag force and can easily gain enough kinetic energy from the fluid to overcome the gravity and inertia force. As the D_p increases, the *Stk* of the particles increases, and the increased drag force is not enough to overcome the exponentially increasing gravity and inertia forces, which makes it difficult for larger particles to escape from the valve chamber.

Due to the great kinetic energy loss of the particles and the gas, the effect of gravity on the deposition rate is gradually highlighted as the particles pass through the valve chamber and enter the horizontal downstream pipe. The values of particle deposition rates for the four VOD are very similar when the D_p is 200 μm. As the D_p increases, the particle deposition rate at each VOD increases. It is worth noting that the deposition is most severe when VOD = 0.75. Observing the streamline of the gas flow at 0.75 opening in Section 5.1.1, it can be seen that the particles are easily pushed towards the top of the pipeline by the gas flow and collide, resulting in energy loss. This directly contributes to the higher deposition rate in the downstream pipe.

5.3. Average erosion rate of valve components

The presence of particles in the chamber and downstream will not only block the flow channel, but also cause the valve components to fail due to the erosion of high velocity particles, which can lead to leakage of the valve. This poses a great challenge to the safe production of shale gas fields. This section summarises and analyses cases 2–5, which investigate the erosion of valve components by VOD and D_p.

The average erosion rate is the sum of the erosion amount of each component and the ratio to the surface area, which responds to the overall erosion of the valve. As shown in Fig. 13., due to the high flow velocity and the high number of direct particle impacts, the average erosion amount of spool is far ahead of the other three components. With the increase of VOD or D_p, the average erosion amount of valve spool tends to increase. Downstream has the lowest average erosion overall.

When the VOD is greater than 0.25, the average erosion of each component at the same VOD is roughly spool-chamber-upstream-downstream from largest to smallest. However, when the VOD is reduced to 0.25, the average erosion rate of each component is different. As shown in Fig. 8(a), at the beginning of the large vortex in the valve chamber, i.e. from the throttle port close to the spool up to the top of the chamber. Since the gravity is vertically downward, the drag force of the gas flow on the particles is opposite to the direction of the gravity, and the kinetic energy of the particles is consumed in the process of reaching the apex of the chamber. Therefore, when VOD = 0.25, with the increase of D_p, gravity also strengthens the reduction of particle kinetic energy. The results show that the average erosion rate in the valve chamber decreased with the increase of D_p. In addition, compared with chamber and downstream, the average erosion rate of upstream under this VOD has generally ushered in a large increase and significantly surpassed that of chamber and downstream. This indicates that smaller VOD are highly susceptible to exacerbating upstream erosion.

5.4. Maximum erosion rate of valve components

The maximum erosion rate serves as a critical parameter, representing the most severe localized material loss, which directly governs the operational lifetime and, crucially, the sealing integrity of components like the valve spool and chamber. Localized perforation or excessive thinning can lead to immediate valve failure.

5.4.1. Effect of particle diameter and VOD on erosion

As shown in Fig. 14., as the D_p increases, the erosion rate of the valve components generally tends to increase. As mentioned in section 5.3.1 the average erosion in the upstream sees a large overall increase when the VOD = 0.25 and significantly exceeds that of the chamber and downstream. This phenomenon also occurs in the result of maximum erosion rate. As shown in the

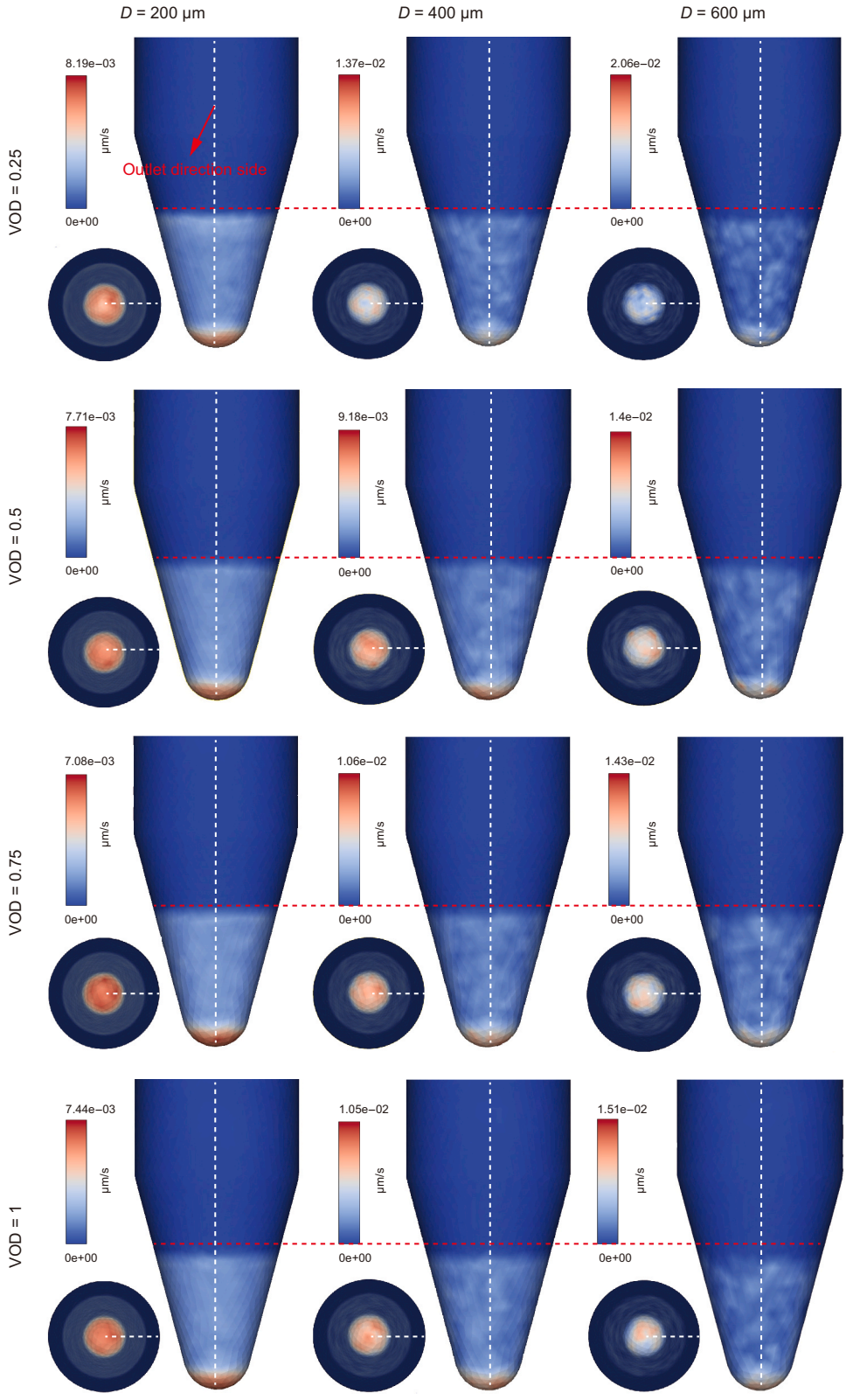

Fig. 17. Contour of downstream erosion rate distribution.

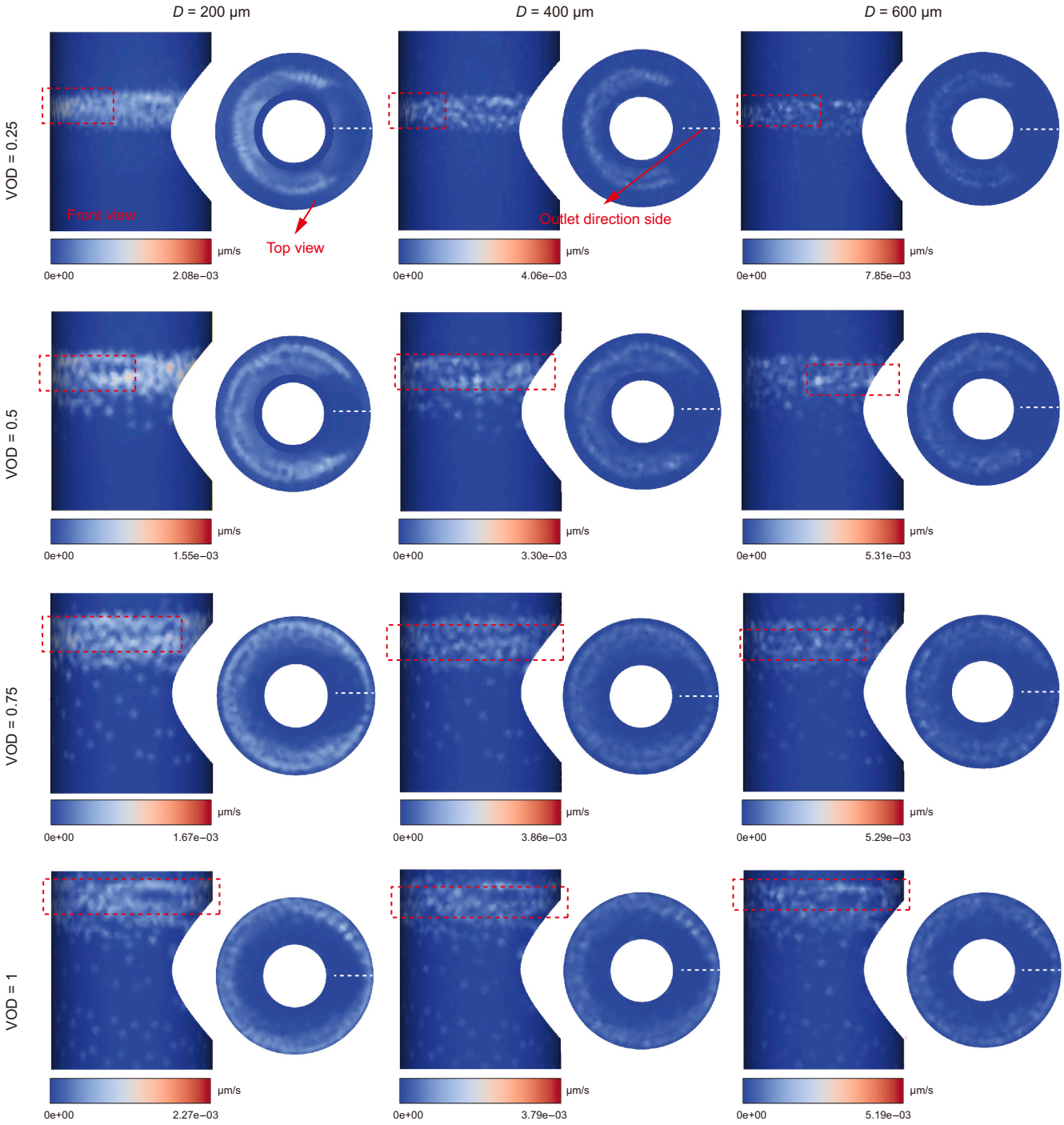

Fig. 18. Contour of valve chamber erosion rate distribution.

following: When the VOD is greater than 0.25, the upstream maintains a small value for both the average and maximum erosion rate. However, when the value of VOD reduces to 0.25, the average and maximum erosion rate of the upstream for different D_p exceeds the corresponding values for chamber and downstream.

Fig. 15 is the contour of upstream pipeline erosion rate distribution, the region of the upstream that is susceptible to erosion damage is concentrated in the top part of upstream, and the closer to the top, the more serious the erosion damage is. Since the most eroded areas of the upstream pipeline are concentrated at the top of the pipeline, a red line is used to indicate where the maximum erosion rate occurs. It is not difficult to find that the erosion area when the VOD = 0.25 is very different from the other VODs. When the VOD = 0.25, a "dense erosion zone" appears near the apex of the upstream pipe (shows in the red dashed box in Fig. 15.). As the D_p increases, the "dense erosion zone" shrinks towards the top of the pipe, and the maximum erosion rate increases.

To figure out the reason for the formation of "dense erosion zone", the trajectory of the particles after impacting the spool when VOD = 0.25 is shown in Fig. 16. From the angle comparison

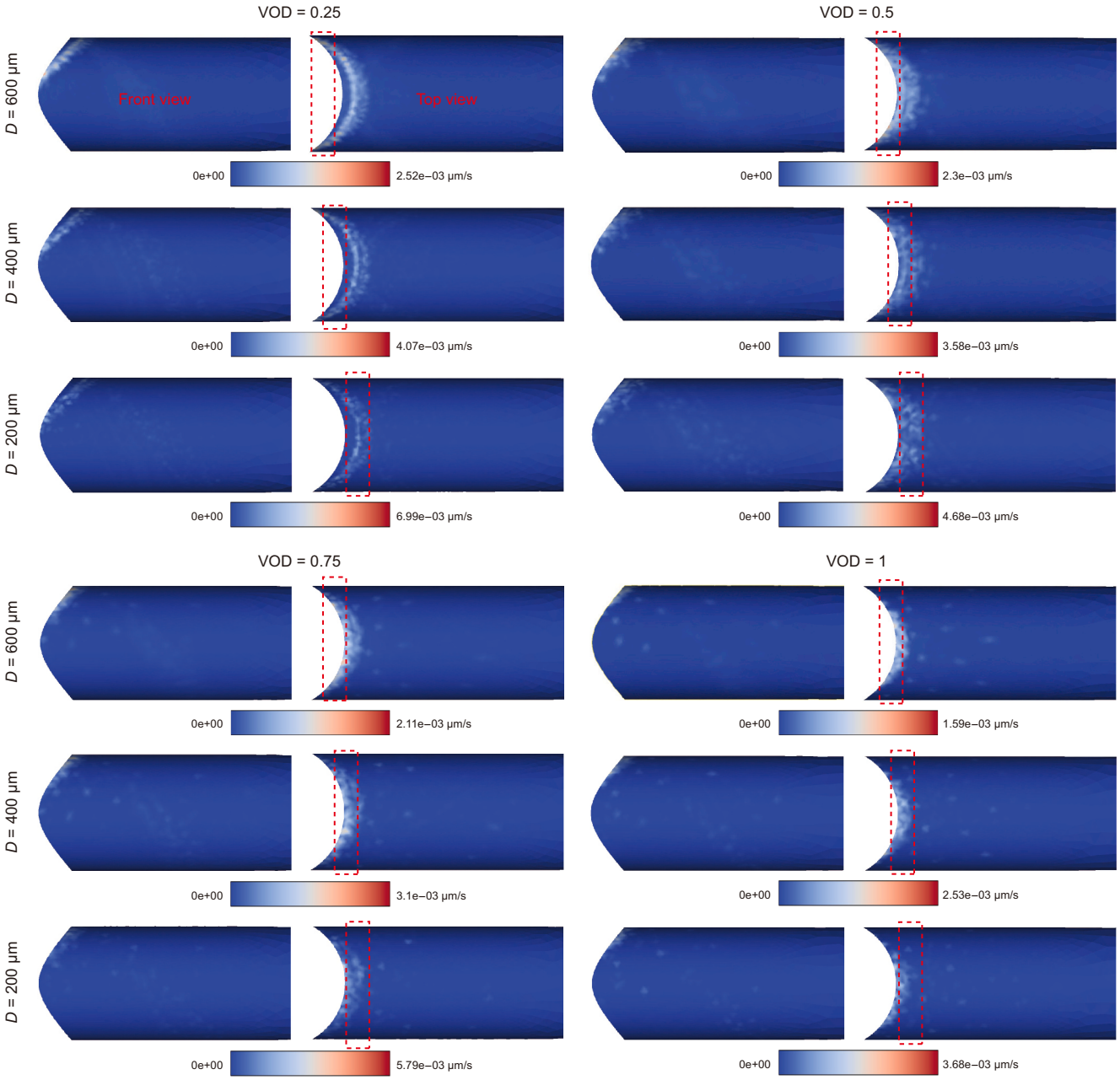

Fig. 19. Contour of downstream erosion rate distribution.

of the red dashed line in the figure ($\theta_3 < \theta_2 < \theta_1$), it can be seen that with the increase of particle diameter, the angle between the extension of the particle trajectory and the upstream wall after the particles impact with the spool gradually decreases. This directly leads to an upward shift in the position of the particle's "secondary collision" with the upstream. This is an important reason why the maximum erosion rate of upstream pipelines increases with the increase in particle diameter.

Combined with sections 5.1.1 and 5.3.1, it is easy to find that compared with the other VODs, when VOD = 0.25, due to the rapid reduction of the flow area of the throttling channel, the particles are extremely easy to collide with the upstream. These collisions directly lead to the maximum erosion rate of the upstream exceeded the chamber and downstream. This indicates that the influence of the smaller VOD on the upstream is greater than that of the chamber and downstream. The influence of particle erosion on the upstream should not be underestimated when the valve is kept in a small VOD for a long period of time.

As shown in Fig. 14., it can be seen that spool is undoubtedly the most susceptible component to erosion under all operating conditions. When VOD = 0.25, there is a large increase in the maximum erosion rate of spool. Fig. 17 is the counter of the spool erosion rate distribution, where the white dashed line represents the direction towards the outlet side. From the contour, it can be found that when the D_p is small, the distribution of particle erosion is more uniform. With the increase of D_p, the eroded area gradually degraded from flake to point. This indicates that the increase in D_p exacerbates the uneven distribution of spool erosion. This results in a large number of erosion pits on the surface of the spool surface, which can greatly damage the airtightness and reduce the structural strength of the spool.

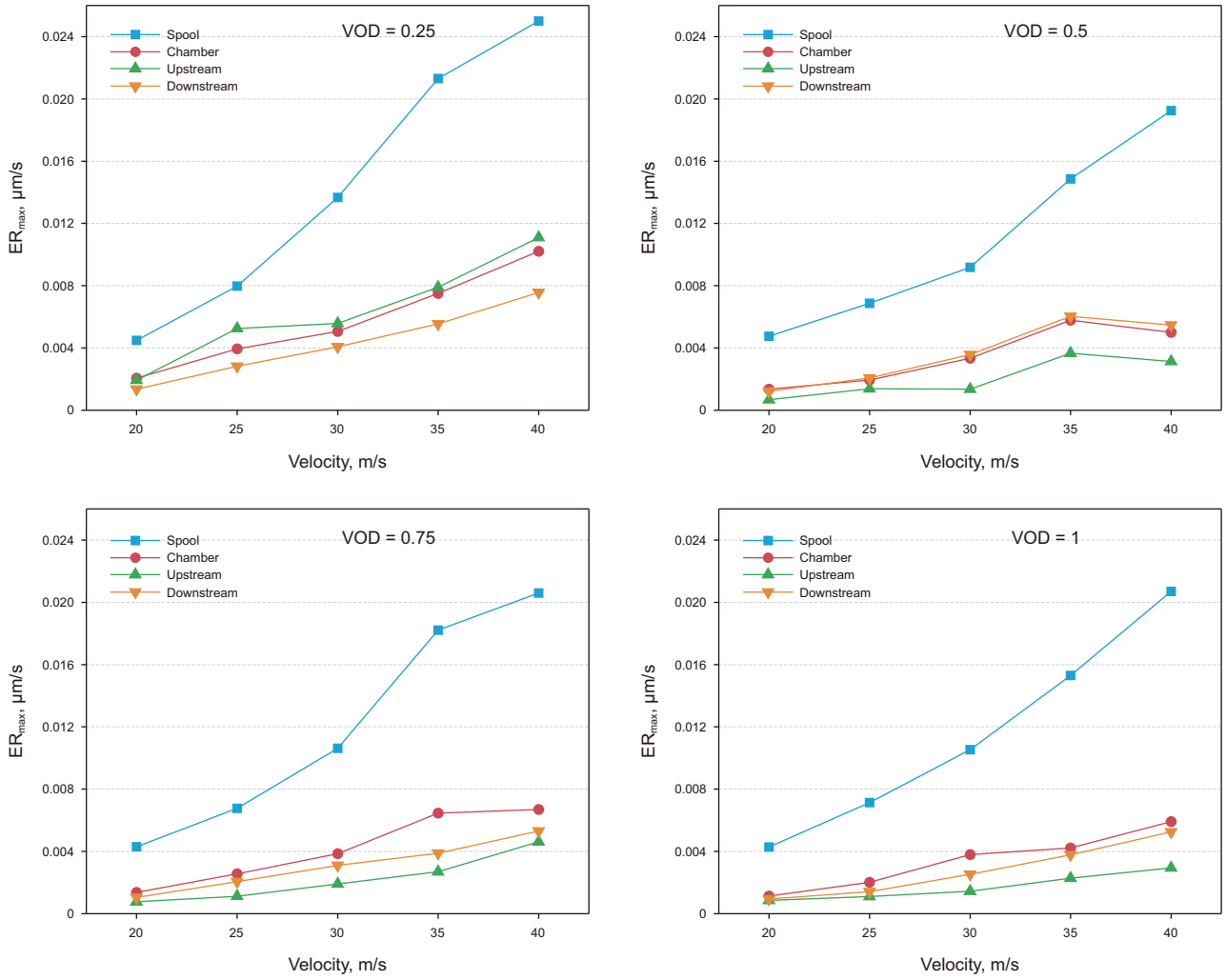

Fig. 20. Flow erosion under different inlet velocities.

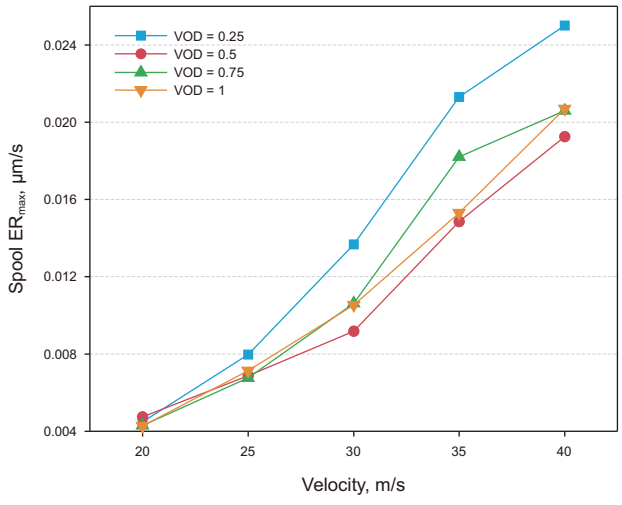

Fig. 21. Variation of maximum erosion at the spool under different inlet velocities.

In addition, the location of the red dashed line in Fig. 17 is the limit where significant erosion occurs. The position of this line hardly moves with the change of VOD and particle diameter, suggesting a well-defined "vulnerable zone" of the spool that occupies 2/3 of the height of the spool cone. When the VOD is 0.25 and the particle diameter is 600 μm, the erosion rate of the spool reaches a maximum value of $2.06e^{-2}$ μm/s. During the design of the valve, the first thing to do is to avoid this area becoming a sealing component of the valve. Apart from that, the spool can be modularized to facilitate the replacement of the "vulnerable zone", thereby extending the overall service life of the spool and reducing the operating costs of the field. In the production process of shale gas field, this region should be focused on flaw detection and inspection.

Fig. 18 is the contour of valve chamber erosion rate distribution, when VOD = 1, the erosion region is evenly dispersed in the side wall and upper wall of the chamber in a dotted shape. The red dotted box in the diagram is where the maximum erosion rate occurs. As the VOD decreases, this region is concentrated in the middle and upper part of the chamber sidewall. Combined with Fig. 8 in Section 5.1.1, it is not difficult to find that the position of the sidewall that is susceptible to erosion and the position of the streamline in the flow field are related to the position of the wall contact point, which is especially obvious when the VOD = 0.25. At the top region of the chamber, a "low erosion rate zone" emerges on the outlet side of the Chamber's upper section as the VOD decreases.

Fig. 19 is the front view and top view of the contour of downstream erosion rate, regions of downstream erosion are generally

concentrated at the top of the pipe near the chamber end. The red dotted box in the diagram is where the maximum erosion rate occurs. The maximum erosion rate decreases with the increase of VOD while increases with the increase of D_p. It is worth noting that when the VOD = 0.25, a "low erosion rate zone" zone appears on the left side of the top of the downstream pipeline. This region is adjacent to the "low erosion rate zone" of the valve chamber. Combined with Fig. 8., it is not difficult to find that due to the effect of the VOD, the gas flow on the right side of the valve chamber forms a low-speed and high-pressure zone in the upper part of the valve chamber. It is precisely because of the presence of this zone that it is difficult for most of the particles to pass directly through this zone to erode the top of the valve chamber and the left side of the top of the downstream pipe.

5.4.2. Effect of inlet velocity on erosion

The inlet velocity is the single external variable most directly correlated with the kinetic energy of the particles, which is the sole determinant of impact damage. High-velocity impacts can transition material response from simple ductile deformation to complex mechanisms involving strain rate hardening or brittle fracture.

In addition to different VOD and D_p, gas flow velocity is also a major variable in the production process of shale gas fields. Cases 6–9 in Table 5 investigate the effect of different inlet velocities on the erosion results.

Fig. 20 demonstrates the impact of varying inlet velocity on the maximum erosion rate. Since the spool is a key throttling component, its maximum erosion rate increases with the inlet velocity and is much higher than the other three components. When VOD is equal to 0.25, 0.5 and 1, the value of the maximum erosion rate in each part of the valve increases synchronously with the increase of the velocity at the inlet. Different from the above three VODs, when the VOD = 0.5, the maximum erosion rate of the chamber, upstream and downstream first increase with the increase of the inlet velocity, and then peak at the inlet velocity of 35 m/s and then decrease. Meanwhile, although the maximum erosion rate of the spool increases with the inlet flow velocity, the value of its maximum erosion rate when the inlet velocity exceeds 25 m/s is significantly smaller than the corresponding value for other VOD, as shown in Fig. 21. This indicates that the 0.5 VOD has a good effect on inhibiting erosion at high flow velocity.

In addition, it is worth noting that the value of maximum erosion rate of upstream when the VOD = 0.5, 0.75 and 1 maintain minimum values at the corresponding speeds. However, when the VOD is equal to 0.25, the value exceeds that of chamber and downstream at the corresponding velocity. This again shows that a small VOD can lead to a significant increase in the maximum erosion rate in the upstream.

The observed maximum erosion rates exceed 0.02 μm/s under some conditions. The sand-carrying capacity and sand diameter of gas extracted from the wellhead is a fluctuating and changing process due to the process and the production cycle of the shale gas field. Due to the great risk of valve failure in shale gas fields, some of the working conditions in this paper are calculated considering the episodic transient extreme conditions that may be encountered in the actual production process. The aim is to investigate the erosion of valves under extreme conditions. In the actual production process, the conditions allow the conditions will often take additional methods to reduce the erosion of particles on the valve (eg, downhole sand consolidation, etc.). An erosion rate of 2 mm per day under extreme conditions necessitates the immediate consideration of highly wear-resistant materials and the implementation of frequent, focused inspection protocols on the identified "vulnerable zone" to maintain operational safety.

6. Conclusions

This study rigorously analyzed the erosion of NTV in shale gas fields, a critical failure mechanism under high-velocity particle flow. By employing a comprehensive CFD-DEM coupling calculation model, we moved beyond traditional methods to systematically investigate the precise effects of particle diameter, inlet velocity, and VOD on the erosion rate of specific valve components. Based on rigorous numerical results, the following specific conclusions were drawn:

(1) The constructed CFD-DEM gas-solid two-phase flow model for the NTV was found to be a highly suitable and accurate method for predicting erosion patterns under the complex, high-velocity conditions of this application. This approach provided the specific, detailed data necessary to identify and quantify erosion rates at a granular level.
(2) The numerical analysis demonstrated a direct and quantifiable relationship between particle diameter and erosion rate. Our simulations showed that the maximum erosion rate of the valve components to increase as the particle diameter increases.
(3) The VOD was identified as a dominant factor in controlling erosion distribution. As the VOD decreases, the erosion rate of the upstream pipeline rises sharply. Meanwhile, the upper part of the side wall of the valve chamber is prone to erosion concentration areas. The best results in suppressing the erosion rate under high flow velocity conditions are obtained when the VOD = 0.5.
(4) Our detailed numerical investigation confirmed that the Spool is the most severely eroded component of the NTV. The simulation data revealed a fixed and well-defined "vulnerable zone" that occupies approximately 2/3 of the height of the spool cone. This finding provides direct guidance for valve design and operation. In the design phase, the sealing surfaces of the valve should be strategically relocated to avoid this identified high-wear region. Operationally, this specific vulnerable zone should be the primary focus of non-destructive flaw detection and maintenance inspections to predict and prevent catastrophic failure.

In conclusion, this study provides specific and quantifiable insights into the erosion failure mechanism of throttle valves through validated numerical simulation methods, and proposes targeted design optimization and operation and maintenance suggestions rather than broad general statements. Future work will leverage these findings by collecting more experimental data and applying data-driven methods to analyze the gas-solid flow in different valve types, thus providing more detailed and guiding suggestions for optimal design and predictive maintenance. We will also perform a deeper analysis of the underlying physics of particle collision effects to further explain the erosion mechanisms identified in this study.

CRediT authorship contribution statement

Bing-Yuan Hong: Writing – review & editing, Writing – original draft, Visualization, Validation, Software, Methodology, Investigation, Formal analysis, Data curation, Conceptualization. **Zhe Wu:** Writing – review & editing, Writing – original draft, Software, Methodology, Investigation, Data curation, Conceptualization. **Yan-Bo Li:** Writing – review & editing, Writing – original draft, Visualization, Methodology, Investigation, Data curation, Conceptualization. **Yu Meng:** Writing – review & editing, Resources, Methodology, Investigation, Formal analysis. **Yue Su:** Writing – review & editing,

Writing – original draft, Investigation, Funding acquisition, Conceptualization. **Wei-Dong Li:** Writing – review & editing, Methodology, Formal analysis, Data curation, Conceptualization. **Bai-Kang Zhu:** Writing – review & editing, Software, Formal analysis, Conceptualization. **Xian-Lei Chen:** Writing – review & editing, Validation, Software, Formal analysis, Data curation. **Wei-Qiang Wang:** Writing – review & editing, Writing – original draft, Visualization, Validation, Methodology, Investigation, Formal analysis, Data curation, Conceptualization. **Dai-Wei Liu:** Conceptualization, Data curation, Investigation, Methodology, Validation, Visualization, Writing – original draft, Writing – review & editing.

Declaration of interests

The authors declare that they have no known competing financial interests or personal relationships that could have appeared to influence the work reported in this paper.

Acknowledge

This study is supported by the Natural Science Foundation of Chongqing, China (CSTB2023NSCQ-MSX0050), “Pioneer” and “Leading Goose” R&D Program of Zhejiang (No. 2025C01152), Zhejiang Provincial Natural Science Foundation of China under Grant (No. LQ23E040004), Zhejiang New Talent Plan of Student’s Technology and Innovation program (No. 2024R411B040) and Science and Technology Project of Daishan County, Zhoushan City (No. 202215).

References

Chen, J., Wang, Y., Li, X., et al., 2015. Reprint of “erosion prediction of liquid-particle two-phase flow in pipeline elbows via CFD–DEM coupling method. Powder Technol. 282, 25–31. https://doi.org/10.1016/j.powtec.2015.05.037.

Cloete S. Johansen T., S., Amini, S., 2015. Grid Independence behaviour of fluidized bed reactor simulations using the two Fluid Model: Effect of particle size. Powder Technol. 269, 153–165. https://doi.org/10.1016/j.powtec.2014.08.055.

Cloete S. Johansen T., S., Amini, S., 2016. Grid independence behaviour of fluidized bed reactor simulations using the Two Fluid Model: Detailed parametric study. Powder Technol. 289, 65–70. https://doi.org/10.1016/j.powtec.2015.11.011.

Gosman, A., Loannides, E., 1983. Aspects of computer simulation of liquid-fueled combustors. J. Energy 7 (6), 482–490. https://doi.org/10.2514/3.62687.

Hong, B., Li, X., Song, S., et al., 2020. Optimal planning and modular infrastructure dynamic allocation for shale gas production. Appl. Energy 261, 114439. https://doi.org/10.1016/j.enpol.2016.12.020.

Hong, B., Li, X., Li, Y., et al., 2021a. Numerical simulation of elbow erosion in shale gas fields under gas-solid two-phase flow. Energies 14 (13), 3804. https://doi.org/10.3390/en14133804.

Hong, B., Li, Y., Li, X., et al., 2021b. Numerical simulation of gas-solid two-phase erosion for elbow and tee pipe in gas field. Energies 14 (20), 6609. https://doi.org/10.3390/en14206609.

Hong, B., Li, Y., Li, X., et al., 2022. Experimental investigation of erosion rate for gas-solid two-phase flow in 304 stainless/L245 carbon steel. Pet. Sci. 19 (3), 1347–1360. https://doi.org/10.1016/j.petsci.2022.01.011.

Hong, B., Li, Y., Li, Y., et al., 2023. Numerical simulation of solid particle erosion in the gas-liquid flow of key pipe fittings in shale gas fields. Case Stud. Therm. Eng. 42, 102742. https://doi.org/10.1016/j.csite.2023.102742.

Jia, W., Zhang, Y., Li, C., et al., 2021. Experimental and numerical simulation of erosion-corrosion of 90 steel elbow in shale gas pipeline. J. Nat. Gas Sci. Eng. 89, 103871. https://doi.org/10.1016/j.jngse.2021.103871.

Knudsen, B.R., Foss, B., 2017. Shale-gas wells as virtual storage for supporting intermittent renewables. Energy Policy 102, 142–144. https://doi.org/10.1016/j.enpol.2016.12.020.

Li, Z., Chen, H., Wu, Y., et al., 2024. CFD-DEM analysis of hydraulic conveying of non-spherical particles through a vertical-bend-horizontal pipeline. Powder Technol. 434, 119361. https://doi.org/10.1016/j.powtec.2024.119361.

Lin, N., Lan, H., Xu, Y., et al., 2015. Effect of the gas–solid two-phase flow velocity on elbow erosion. J. Nat. Gas Sci. Eng. 26, 581–586. https://doi.org/10.1016/j.jngse.2015.06.054.

Lin, N., Arabnejad, H., Shirazi, S., et al., 2018. Experimental study of particle size, shape and particle flow rate on Erosion of stainless steel. Powder Technol. 336, 70–79. https://doi.org/10.1016/j.powtec.2018.05.039.

Lin, Z., Sun, X., Yu, T., et al., 2020. Gas–solid two-phase flow and erosion calculation of gate valve based on the CFD-DEM model. Powder Technol. 366, 395–407. https://doi.org/10.1016/j.powtec.2020.02.050.

Lin, Z., Sun, X., Li, Y., et al., 2022. Numerical study of gas–solid two-phase flow and erosion in a cavity with a slope. Particuology 62, 25–35. https://doi.org/10.1016/j.partic.2021.05.010.

Mazur, Z., Campos-Amezcua, R., Urquiza-Beltrán, G., et al., 2004. Numerical 3D simulation of the erosion due to solid particle impact in the main stop valve of a steam turbine. Appl. Therm. Eng. 24 (13), 1877–1891. https://doi.org/10.1016/j.applthermaleng.2004.01.001.

Menter, F.R., 1994. Two-equation eddy-viscosity turbulence models for engineering applications. AIAA J. 32 (8), 1598–1605. https://doi.org/10.2514/3.12149.

Morsi, S., Alexander, A., 1972. An investigation of particle trajectories in two-phase flow systems. J. Fluid Mech. 55 (2), 193–208. https://doi.org/10.1017/S0022112072001806.

Neilson, J., Gilchrist, A., 1968. Erosion by a stream of solid particles. Wear 11 (2), 111–122. https://doi.org/10.1016/0043-1648(68)90591-7.

Oka, Y.I., Okamura, K., Yoshida, T., 2005. Practical estimation of erosion damage caused by solid particle impact: part 1: effects of impact parameters on a predictive equation. Wear 259 (1–6), 95–101. https://doi.org/10.1016/j.wear.2005.01.039.

Oka, Y., Yoshida, T., 2005. Practical estimation of erosion damage caused by solid particle impact: Part 2: Mechanical properties of materials directly associated with erosion damage. Wear 259 (1–6), 102–109. https://doi.org/10.1016/j.wear.2005.01.040.

Raffel, M., Willert, C.E., Scarano, F., et al., 2018. Particle Image Velocimetry: A Practical Guide. Springer International Publishing. https://doi.org/10.1007/978-3-319-68852-7.

Tan, H., Wong-Parodi, G., Zhang, S., et al., 2022. Public risk perceptions of shale gas development: A comprehensive review. Energy Res. Social Sci. 89, 102548. https://doi.org/10.1016/j.erss.2022.102548.

Vieira, R.E., Mansouri, A., McLaury, B.S., et al., 2016. Experimental and computational study of erosion in elbows due to sand particles in air flow. Powder Technol. 288, 339–353. https://doi.org/10.1016/j.powtec.2015.11.028.

Wallace, M., Dempster, W., Scanlon, T., et al., 2004. Prediction of impact erosion in valve geometries. Wear 256 (9–10), 927–936. https://doi.org/10.1016/j.wear.2003.06.004.

Wang, Q., Huang, Q., Wang, N., et al., 2021. An experimental and numerical study of slurry erosion behavior in a horizontal elbow and elbows in series. Eng. Fail. Anal. 130, 105779. https://doi.org/10.1016/j.engfailanal.2021.105779.

Wang, Z., Zhang, J., Shirazi, S.A., et al., 2019. Predicting erosion in a Non-Newtonian shear-thinning jet flow with validated CFD models from PIV and PTV measurements. Wear 426, 501–506. https://doi.org/10.1016/j.wear.2018.12.027.

Willert, C.,S., Wereley, T., Kompenhans, J., 2018. In: Particle Image Velocimetry, third ed. Springer International Publishing. https://doi.org/10.1007/978-3-319-68852-7.

Wu, Z., Wang, C., Lang, R., et al., 2024. The distribution of components in hydrogen-blended pipelines under different gas stream injection pattern. Fuel 375, 132577. https://doi.org/10.1016/j.fuel.2024.132577.

Xu, B., Lin, Z., Zhu, Z., et al., 2022. Experimental and simulation study of the effect of gravity on the solid-liquid two-phase flow and erosion of ball valve. Adv. Powder Technol. 33 (2), 103416. https://doi.org/10.1016/j.apt.2021.103416.

Xu, L., Zhang, Q., Zheng, J., et al., 2016. Numerical prediction of erosion in elbow based on CFD-DEM simulation. Powder Technol. 302, 236–246. https://doi.org/10.1016/j.powtec.2016.08.050.

Zhang, P., Zheng, S., Jing, J., et al., 2015. Surface erosion behavior of an intrusive probe in pipe flow. J. Nat. Gas Sci. Eng. 26, 480–493. https://doi.org/10.1016/j.jngse.2015.05.037.

Zhou, Z., Kuang, S., Chu, K., et al., 2010. Discrete particle simulation of particle–fluid flow: Model formulations and their applicability. J. Fluid Mech. 661, 482–510. https://doi.org/10.1017/S002211201000306X.

Zhu, H., Pan, Q., Zhang, W., et al., 2014. CFD simulations of flow erosion and flow-induced deformation of needle valve: effects of operation, structure and fluid parameters. Nucl. Eng. Des. 273, 396–411. https://doi.org/10.1016/j.nucengdes.2014.02.030.

Zhu, H., Qi, Y., 2019. Numerical investigation of flow erosion of sand-laden oil flow in a U-bend. Process Saf. Environ. Prot. 131, 16–27. https://doi.org/10.1016/j.psep.2019.08.033.